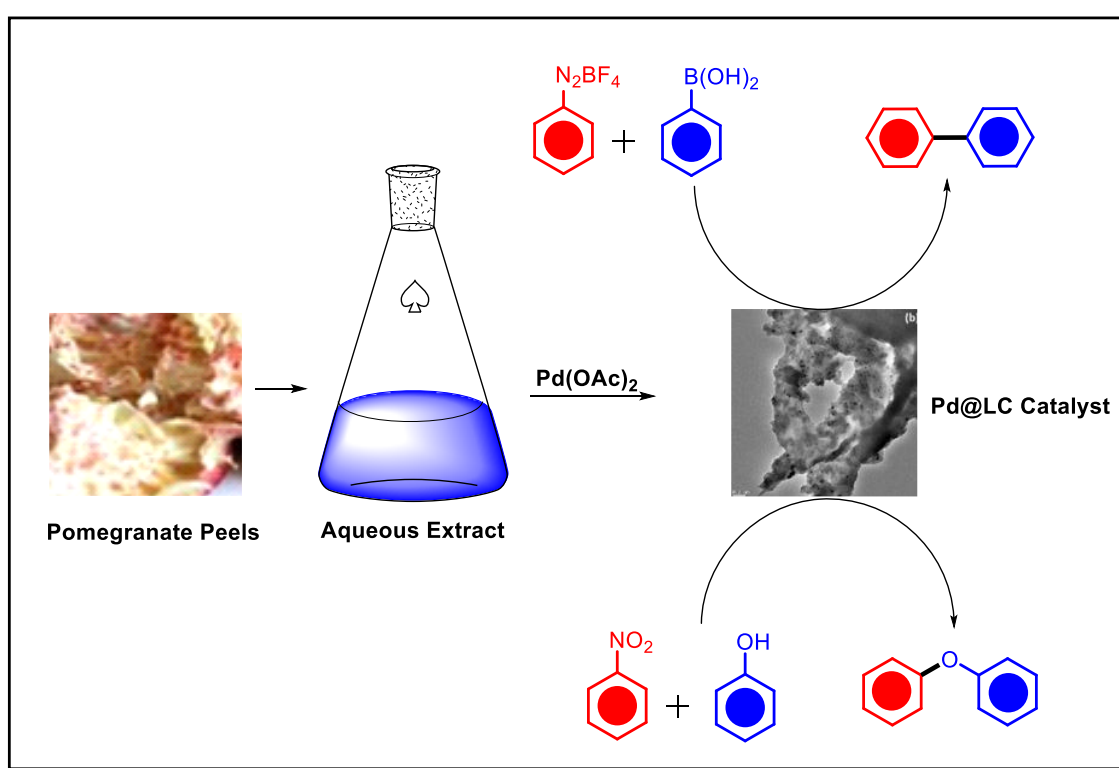


Chapter 3

Utilising Palladium (0)-Supported Lignocellulosic Biomass Catalyst for C-C and C-O Bond Formations

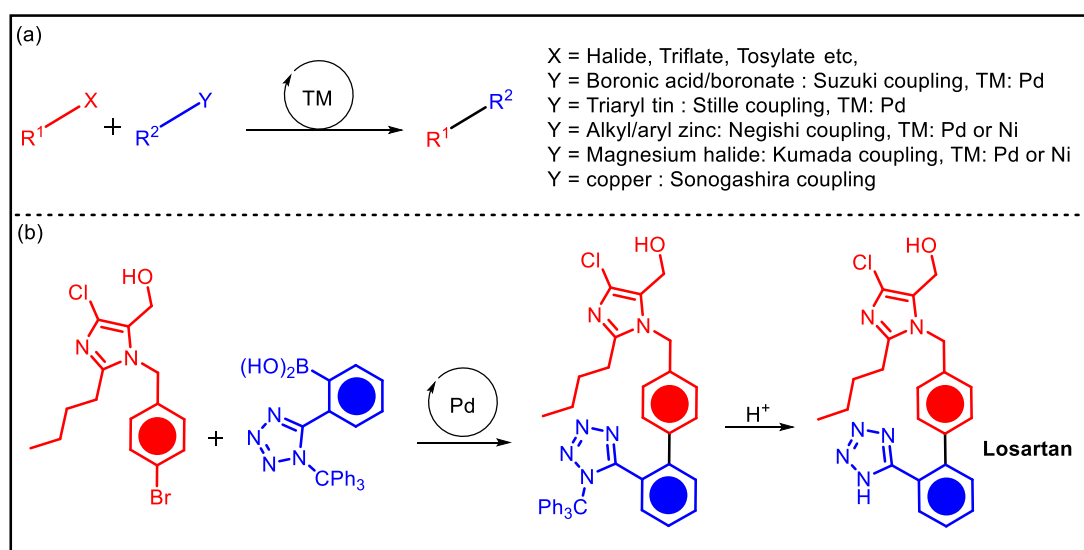


Abstract: Derived from discarded pomegranate peels, lignocellulose has been repurposed as an eco-friendly and carbon-neutral resource, serving as a foundational material for palladium nanoparticles. This transformation was achieved through a straightforward aqueous extraction method that maintained its natural structure, as evidenced by TEM analysis. The system efficiently facilitated the Suzuki-Miyaura cross-coupling of aryl diazonium tetrafluoroborates with arylboronic acids as well as the de-nitrative cross-coupling of aryl nitrates with phenols to form diaryl ethers.

Utilising Palladium (0)-Supported Lignocellulosic Biomass Catalyst for C-C and C-O Bond Formations

3.1. Introduction

Cross-coupling reactions, one of the most versatile organic reactions, have emerged as expedient tools for the generation of carbon-carbon and carbon-heteroatom linkages which has tremendously helped in pharmaceuticals, agrochemicals, and material science [1]. This includes carbon-carbon forming processes such as Suzuki-Miyaura, Mizoroki-Heck, Buchwald-Hartwig, Negishi, Chan-Lam processes and many more. The discovery of such reactions has made the formation of bonds which were earlier considered to be non-feasible [3]. This has significantly helped in the synthesis of privileged scaffolds and APIs. For example, the synthesis of antihypertensive drugs Losartan and Valsartan involves a late-stage palladium catalysed Suzuki coupling (Scheme 3.1) [4], the synthesis of the anticoagulant Apixaban involves a crucial Chan-Lam amination etc [5]. The term cross-coupling refers to the joining of two functionalised fragments to form a single molecule in the presence of a transition metal catalyst [6]. Although, several transition metals can facilitate cross-coupling reactions, the scene is dominated by palladium. Roughley and Jordan reported that 62% of all cross-coupling based carbon-carbon bond forming processes utilised for preparing drugs and APIs are predominantly palladium catalysed [6].



Scheme 3.1. Transition metal catalysed cross-couplings; b) Suzuki-Miyaura cross-coupling in the synthesis of Losartan

Palladium, a *4d* transition metal and its salts are the most exploited catalysts for cross-coupling reactions [7]. Its versatility lies in the easy switching of oxidation states involving the Pd(0)/Pd(II) couple and high functional group tolerance. This in turn has made it highly essential industrially [8]. Most of the homogeneous cross-coupling mechanisms involving palladium salts rely on the initial generation of Pd(0) to facilitate oxidative addition processes. However, the usage of homogeneous palladium catalysts suffers from disadvantages such as toxicity, poisoning, requirement of expensive ligands, difficulties related to separation and reusability issues [9, 10, 11]. To solve some of such problems, a lot of effort has been given to the development of supported palladium catalysts. Such catalysts consist of palladium (mostly nanosized) dispersed over solid supports. These materials are seen to be robust and reusable in cross-coupling reactions with high product yields. Supports for palladium nanoparticles can be metal oxides, metal/covalent organic frameworks, cellulosic materials as well as bio-based supports. All these materials have advantages of their own.

3.1.1. Suzuki-Miyaura cross-coupling.

Of the cross-coupling reactions involving palladium catalysis, Suzuki coupling of organohalides with arylboronic acids/boronates has become a basic transformation in organic molecule synthesis [12]. This reaction requires catalytic palladium in the presence of a base whose role is to activate the boronic acid/boronate and provides biaryls in excellent yields. The high degree of reproducibility, good functional group tolerance, non-requirement of inert atmospheres and non-toxicity of boronic acid derivatives are the major pros in the reaction. However, designing heterogeneous catalytic systems for Suzuki-Miyaura cross-coupling reaction for long term sustainability is relevant. An important approach for the same is to develop catalysts that can be recycled for multiple cycles without significant catalytic efficacy loss [13].

3.1.2. De-nitrative cross-coupling

Nitroarenes serve as abundant chemical feedstocks, with their de-nitrative transformations being highly valuable in synthetic chemistry due to the ease of preparing nitroarenes from simple starting materials through electrophilic aromatic nitration [14]. As synthetic intermediates, nitro compounds allow access to

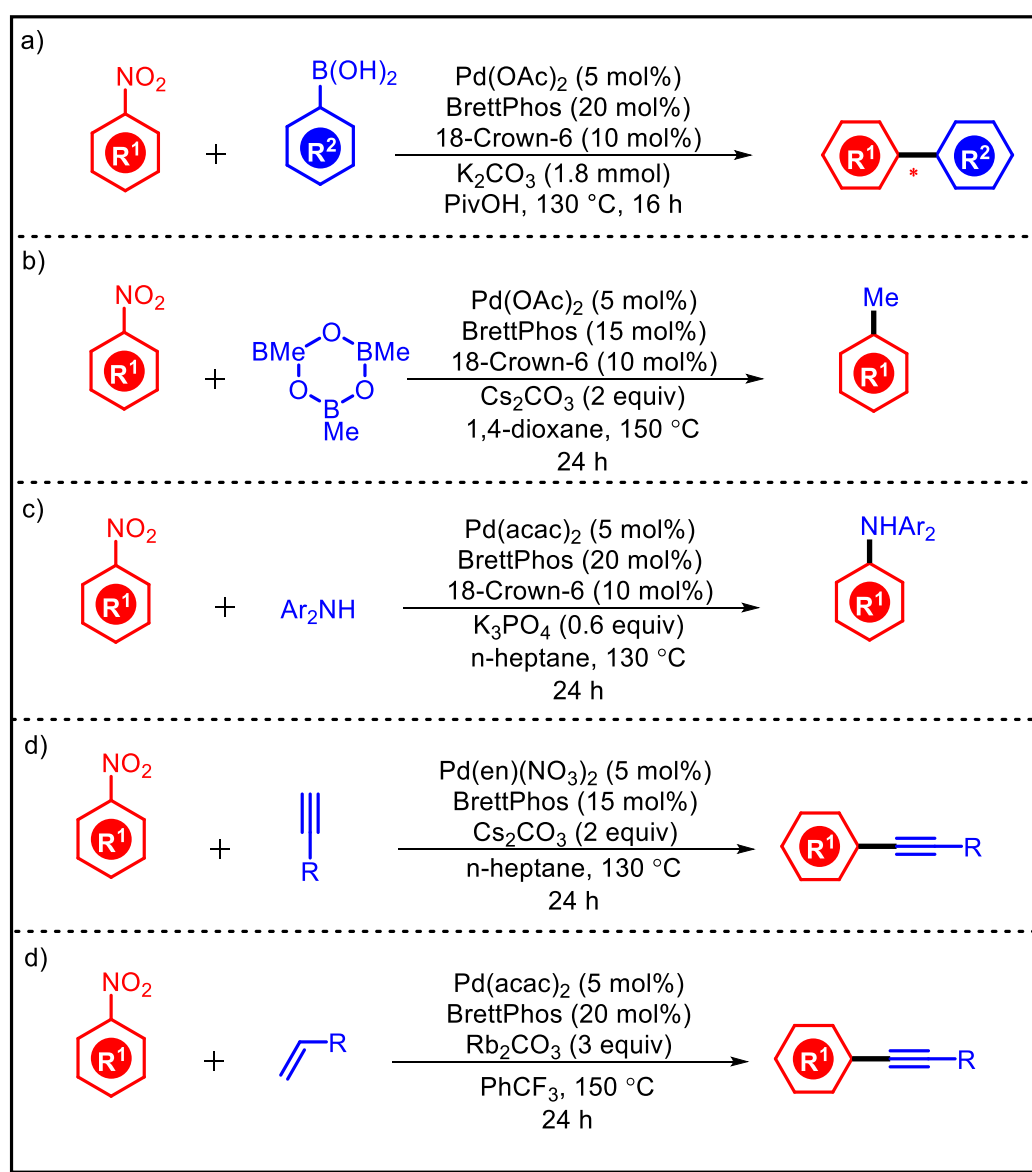
haloarenes *via* reduction, diazotisation, and halogenation, and are also used in the synthesis of heterocyclic compounds. The electron-withdrawing nature of the nitro group makes it a temporary leaving group, facilitating conversion to other important functional groups [14].

The traditional reactions involving de-nitration are usually achieved *via* nitro to amino reduction. The direct oxidative addition of nitroarene to a metal center would therefore provide newer avenues in organic synthesis. Interestingly, the use of nitroarenes in cross-coupling were limited due to the absence of an effective metal catalyst to efficiently break the C–NO₂ bond. While the C–NO₂ bond is relatively inert toward transition metal catalysts, the –NO₂ group often deactivates these catalysts, presenting challenges for developing de-nitrative transformations. However, the use of palladium as a central metal in combination with BrettPhos as a ligand enabled the groundbreaking oxidative addition of Ar–NO₂ bonds to Pd(0) [14a, 15]. The Pd(II) BrettPhos combination is effective in de-nitrative Suzuki, methylation, amination, Sonogashira and Heck reactions (**Scheme 2**) [15, 16, 17, 18, 19].

While coupling reactions have significantly enriched our understanding of nitroarene chemistry, substantial scope remains for expanding their synthetic utility. A particularly promising direction involves the use of heterogeneous catalytic systems to facilitate de-nitrative carbon–carbon (C–C) and carbon–heteroatom (C–X) bond-forming reactions. These systems not only offer the potential for enhanced efficiency and selectivity but also align well with principles of green chemistry through improved sustainability, catalyst reusability, and operational simplicity.

In this context, bio-supported nanomaterials—especially those derived from renewable biomass—have gained considerable attention. Among them, lignocellulosic biomass stands out as a versatile and eco-friendly support material. It is composed of three major biopolymers: cellulose, hemicellulose, and lignin [20], which are intricately woven into a complex, non-uniform three-dimensional matrix that varies across biological sources [21]. This structural diversity, combined with a high density of functional groups and large surface area, makes lignocellulosic materials particularly well-suited for stabilising and dispersing metal nanoparticles in heterogeneous catalytic systems.

Beyond their structural advantages, lignocellulosic supports also offer mechanical robustness, biodegradability, and compatibility with environmentally benign processing methods—factors that make them attractive for sustainable catalyst design. As interest grows in integrating biomass valorisation with advanced catalysis, researchers are increasingly investigating how the individual biopolymeric components influence catalytic behavior. Consequently, current research efforts largely focus on the selective separation of lignocellulose into its three fundamental constituents to better understand and optimise their roles in catalytic applications [22].



Scheme 3.2. Palladium catalysed de-nitrative transformations

However, achieving this separation is challenging, as the structure is naturally designed to resist degradation. This resilience is due to cellulose's crystallinity, the hydrophobic nature of lignin, and the encapsulation of cellulose within a lignin-hemicellulose matrix [20]. Therefore, various pre- and post-treatment processes are necessary to modify the binding properties and physical and chemical characteristics of the lignocellulosic matrix. Despite its abundance and low cost, the primary challenge remains in scaling up these processes, as biomass pretreatment demands high energy, extensive chemical use, severe conditions, and multiple steps, raising questions of sustainability. Thus, the focus is to develop efficient support materials through methods that are both environmentally sustainable and scalable for industrial applications.

3.2. Objectives of the present work

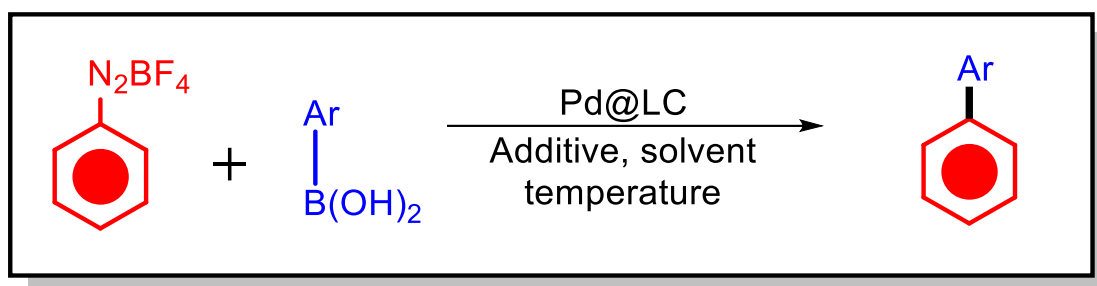
Pomegranate (*Punica granatum*) is a tropical fruit known for its wide array of physiological and nutritional benefits, and its byproducts—particularly the peel—have attracted increasing attention for their potential applications in sustainable materials and bioresource utilisation. A detailed compositional study analysing the fiber content from the peels of 12 different pomegranate varieties revealed a consistently higher proportion of lignin compared to cellulose across all samples. Specifically, lignin content was found to range from 20.59% to 41.86%, significantly surpassing the cellulose content, which varied between 16.53% and 22.71% per hundred grams of fiber. This lignin-rich profile positions pomegranate peel as a promising biomass source for applications where rigidity, thermal stability, or hydrophobicity imparted by lignin is advantageous. This motivated our research group to utilise pomegranate peel fibers as support for palladium nanoparticles to form the catalyst Pd@LC which was found to be excellent to arylate indoles at C2 position with arylboronic acids [23]. Herein, we have synthesised a pomegranate peel base lignocellulose supported palladium nanoparticle catalyst and used it in two important organic transformations (**Chapter 3a** and **3b**) given below:

- Chapter 3a deals with the preparation of the catalyst and its utilisation in the Suzuki-Miyaura type cross-coupling of aryl diazonium salts with aryl boronic acids under external base-free conditions to form biphenyls.

- Chapter 3b deals with the utilisation of the catalyst in the de-nitrative cross-coupling of nitroarenes with phenols to form diaryl ethers.

Chapter 3a

Utilising Palladium (0)-Supported Lignocellulosic Biomass Catalyst for Suzuki-Miyaura Type Cross-Coupling of Aryl Diazonium Salts with Arylboronic acids



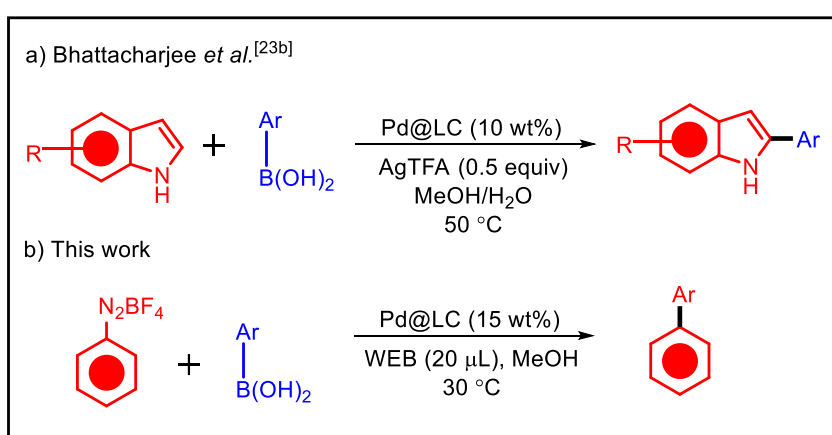
Abstract: Lignocellulose, obtained from discarded pomegranate peels, has been transformed into an environmentally friendly, carbon-neutral material used as a support for palladium nanoparticles. This was accomplished through a simple aqueous extraction process that preserved its natural structure, as confirmed by TEM analysis. The resulting system effectively enabled the Suzuki-Miyaura cross-coupling reaction between aryl diazonium tetrafluoroborates and arylboronic acids.

Utilising Palladium (0)-Supported Lignocellulosic Biomass Catalyst for Suzuki-Miyaura Type Cross-coupling of Aryl Diazonium Salts with Arylboronic acids

3.3. Introduction

The union of nanoparticle tech with materials having porosity is an intriguing and swiftly advancing field of research [24, 25]. The process of affixing and fixing nanoparticles onto a solid foundation allows for meticulous manipulation of their dimensions, structure, and functionality, along with the establishment of distinct adsorption sites [26, 27]. While the scientific community has traditionally been captivated by supported metal nanoparticles, the last ten years have seen the rise of many encouraging biomass and biomass-derived materials [28].

The cross-coupling of aryl diazonium salts with arylboronic acids represents an alternate tactic to the conventional Suzuki-Miyaura reaction. Aryl diazonium salts can be easily prepared from aryl amines with the use of organic and inorganic nitrites at low temperatures. Their inherent reactivity arises due to the tendency of quick removal of nitrogen gas to generate an electrophilic species. This property therefore, has been used in cross-coupling reactions that do not require ligands [29]. Initially reported with aryl stannates, the cross-coupling of aryl diazoniums have been expanded to activated alkenes, terminal alkynes and arylboronic acids [30].



Scheme 3.3. Pd@LC catalysed C-C bond formations

Bora and team recently reported an effective C2-arylation of indoles using aryl boronic acids, employing a catalyst composed of palladium nanomaterial supported

on waste pomegranate peel-derived lignocellulose (**Scheme 3.3(a)**) [23]. In this work, we demonstrate the successful synthesis of the biphenyl system through a Suzuki–Miyaura cross-coupling reaction between aryl boronic acids and aryl diazonium tetrafluoroborates, utilising the same catalyst. Notably, the catalyst is heterogeneous and exhibits the ability to be reused for multiple cycles.

3.4. Experimental Section

3.4.1. General Information

All starting materials (except the diazonium salts) were commercially purchased and used without further purification. The reactions were conducted in Eyela™ process station (EPS) synthesiser tubes under ambient aerial conditions. TLC plates (Silica gel 60-F254 coated on aluminium plates from Merck) were visualised by either UV light or inside an iodine chamber. ^1H and ^{13}C NMR experiments were carried out using JEOL ECS 400MHz and Bruker Avance III 500 MHz and Bruker Avance III 600 MHz spectrometers, with chemical shifts referenced to tetramethyl silane (for ^1H) and CDCl_3 (for ^{13}C NMR) as internal standards. Purification of all products was achieved through column chromatography.

3.4.2. General procedure for the synthesis of lignocellulose supported palladium catalyst.

The peel residue (20 g) obtained from pomegranate fruit was thoroughly washed, finely crushed, ground, and combined with 100 mL of distilled water in a beaker. Subsequently, 10 mL of the resulting aqueous peel suspension was placed in a round bottom flask, and 50 mM (0.112 g) $\text{Pd}(\text{OAc})_2$ was added at room temperature. The change in colour from brown to black signalled the formation of Pd NPs. The reaction mixture was stirred under a nitrogen atmosphere for 48 hours (**Figure 3.1**). The nanomaterials formed were separated from the solution through centrifugation, washed with H_2O , dried under vacuum, and ultimately crushed into fine powdered black materials, identified as Pd@LC. Notably, no biomass pre-treatments or chemical reducing agents were employed in this process. The inherent porosity and the presence of high-density hydrophilic functional groups, such as carbonyl, hydroxyl, and carboxyl groups, make lignocellulose material an effective capping agent for anchoring and stabilising noble nanomaterials on the bio-support.

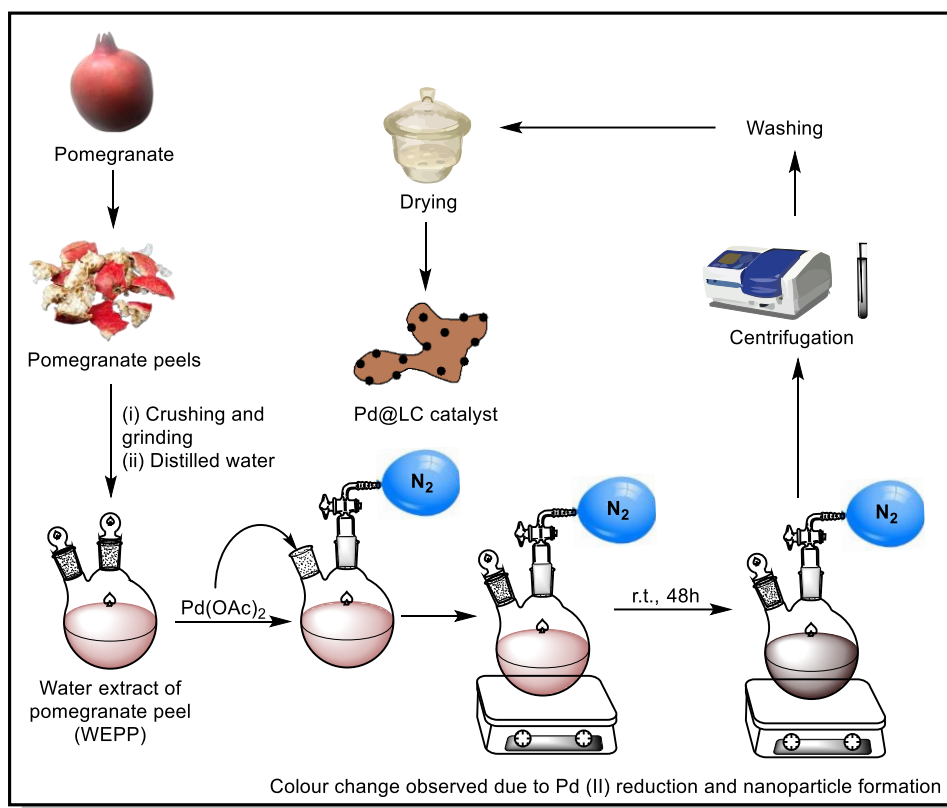


Figure 3.1. Synthesis of Pd@LC catalyst

3.4.3. General procedure for the synthesis aryldiazonium tetrafluoroborates.

In ethanol (5 mL), a solution comprising tetrafluoroboric acid (HBF₄, 1.3 mL) and aromatic amine (5 mmol) was combined, and ^tBuONO (1.4 mL) was added dropwise at 0 °C. The reaction mixture was stirred for 30 minutes at room temperature. After the reaction was complete, diethyl ether (20 mL) was introduced to the mixture, resulting in the precipitation of the respective diazonium salts. The crude mixture underwent filtration, and the residue was washed with diethyl ether (3 X 10 mL) and left to air dry.

3.5. Results and discussion

3.5.1. Characterisation of the synthesised nanomaterial

The low-resolution transmission electron microscopy (TEM) images of Pd@LC (depicted in **Figure 3.2 (a–c)**) reveal the notable presence of Pd NPs intricately intertwined within the lignocellulose bio-network, effectively stabilising their dispersion. The particle size distribution curve (illustrated in **Figure 3.2 (e)**) indicates the uniform size of the Pd NPs embedded in the biomass support,

approximately 9.490 nm in diameter. High-resolution TEM (HRTEM) images of the Pd NPs (depicted in **Figure 3.2 (d)**) demonstrate the existence of lattice fringes with spacings of 0.118 nm and 0.136 nm, aligning with the crystallographic planes of Pd, specifically (220), and (311), respectively.

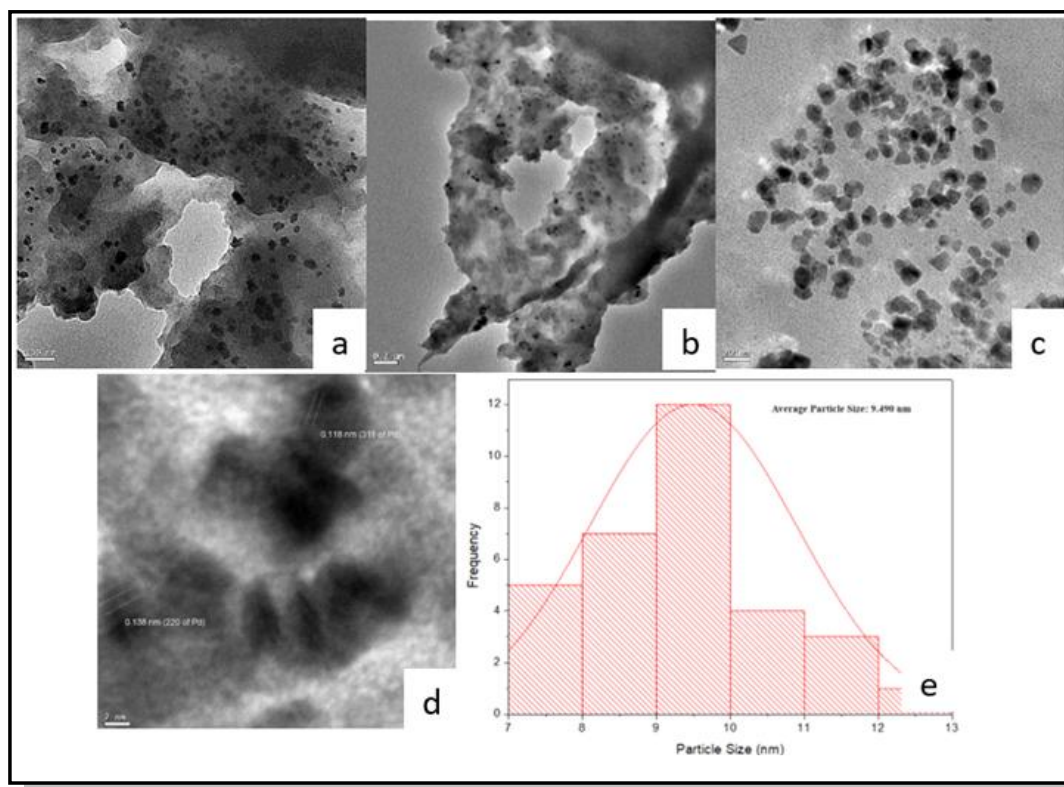


Figure 3.2. *a-d)* TEM images of the nanomaterial; *e)* Particle size distribution

3.5.2. Optimisation of the reaction conditions

Our investigation began by selecting 4-methoxyphenyldiazonium tetrafluoroborate (**1a**) and phenylboronic acid (**2a**) as the model substrates to determine the most favourable reaction conditions. The results of our screening experiments, including variations in substrate ratios, catalyst quantities, additives, solvents, and critical parameters like temperature, are presented in Table 1. Initially, we conducted the reaction between equimolar amounts of **1a** and **2a** in the presence of a 5 wt% catalyst in a methanol medium at 30 °C, resulting in a 65% yield of the desired product (**3a**) (**Table 3.1, Entry 1**). Maintaining all conditions, the same, except for increasing the amount of **2a** to 1.2 equivalents, yielded **3a** with a 69% yield (**Table 3.1, Entry 2**). Further increasing the quantity of **2a** to 1.5 equivalents led to an improved product yield of 72% in a shorter reaction time (**Table 3.1, Entry 3**). Subsequently, raising the

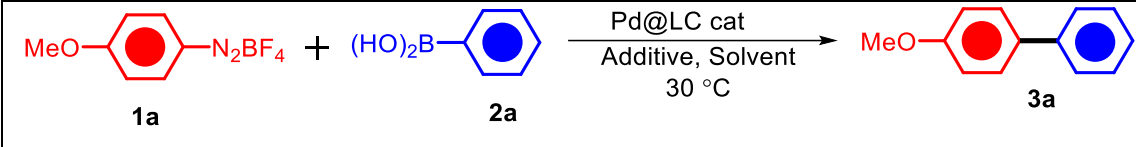
catalyst amount to 10 wt% resulted in a product yield of 76% within 70 minutes (**Table 3.1, Entry 4**). This yield further improved to 86% when 15 wt% of the catalyst was used (**Table 3.1, Entry 5**). The addition of 0.5 equivalents of K_2CO_3 as an additive, while keeping all other parameters constant as in **Entry 5**, led to a rise in product yield to 90%. This increase might be attributed to the additional activation of the boronic acid by potassium carbonate. A similar yield of 91% was achieved by using 20 microliters of WEB (water extract of banana peel ash, pH = 12) as an additive. The presence of carbonate ions in WEB can further activate the boronic acid to facilitate an effective aryl group transfer (**Table 3.1, Entries 6 and 7**). For optimal conversion, a temperature of 30 °C was found to be necessary. When the reaction was carried out at room temperature, the product yield decreased to 84% (**Table 3.1, Entry 8**). Using ethanol and water as solvents led to further decreases in yield to 85% and 40%, respectively. The reduction in product yield with water as a solvent may be attributed to the lower solubility of the starting materials in a water medium (**Table 3.1, Entries 9 and 10**). Utilising a 1:1 mixture of methanol and water as the solvent system yielded a reduced yield of 80% (**Table 3.1, Entry 11**). Finally, the optimised reaction conditions can be summarised as follows: 4-Methoxyphenyldiazonium tetrafluoroborate (**1a**, 1 equiv., 0.5 mmol), Phenylboronic acid (**2a**, 1.5 equiv., 0.75 mmol), Pd cat. (15 wt%), Additive (WEB, 20 μ L), Solvent (MeOH, 4 mL), Temperature (30 °C).

3.5.3. General procedure for Suzuki-Miyaura type cross-coupling reaction.

A thoroughly cleaned and dried synthesiser tube (Eyela™) with a magnetic stirring rod was charged with 1 equiv. (0.5 mmol) of the aryldiazonium salt, 1.5 equiv. (0.75 mmol) of the aryl boronic acid, 15 wt% of the Palladium catalyst, 20 mL of the additive (WEB) in 4 mL methanol solvent. The system was warmed to 30 °C and the reaction mixture was allowed to stir. The progress of the reaction was monitored using TLC. After the completion of the reaction, the reaction mixture was filtered through a plug of celite under pressure and was subjected to solvent extraction using ethyl acetate-water system, treated with brine solution. The combined organic layers were then dried using sodium sulfate and was concentrated in vacuum to obtain the crude product. The purification of the product was done using column chromatography (60-

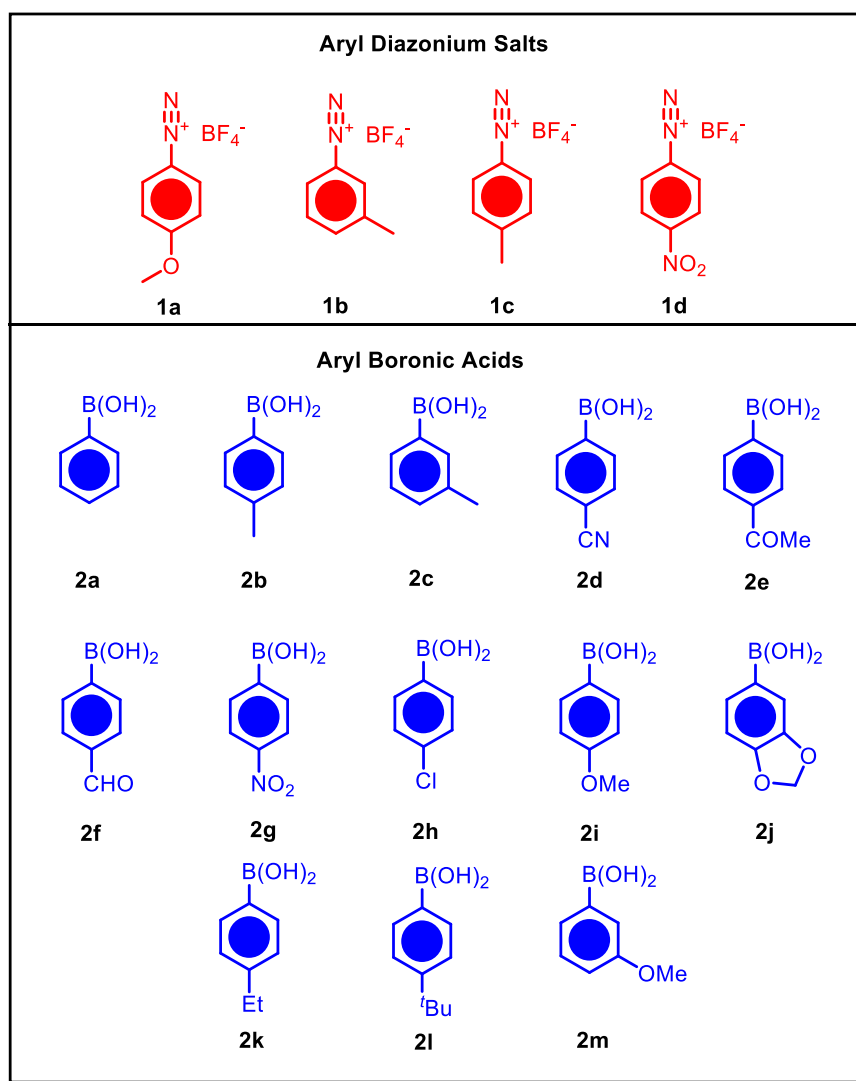
120 mesh silica) with 0-5% ethyl acetate/hexanes as solvent system to obtain the pure product.

Table 3.1. Optimisation of the reaction conditions

							
Sl. No.	1a (mmol)	2a (mmol)	Pd Cat (wt%)	Base	Solvent (4 mL)	Time (h)	Yield (%)
1	0.5	0.5	5	-	MeOH	1.5	65
2	0.5	0.6	5	-	MeOH	1.5	69
3	0.5	0.75	5	-	MeOH	1.25	72
4	0.5	0.75	10	-	MeOH	70 min	76
5	0.5	0.75	15	-	MeOH	1 h	86
6	0.5	0.75	15	K ₂ CO ₃ (0.5eq)	MeOH	1 h	90
7	0.5	0.75	15	WEB (20 µL)	MeOH	1 h	91
8	0.5	0.75	15	WEB (20 µL)	MeOH	1 h	84 ^[a]
9	0.5	0.75	15	WEB (20 µL)	EtOH	1.5 h	85
10	0.5	0.75	15	WEB (20 µL)	H ₂ O	1 h	40
11	0.5	0.75	15	WEB (20 µL)	MeOH:H ₂ O (1:1)	1 h	80
^[a] The reaction was carried out at room temperature							

3.5.4. Substrate Scope Studies

With the optimised conditions in place, our objective was to investigate the compatibility of the refined reaction with various arylboronic acids and diazonium salts.

Table 3.2a. Aryl diazonium salts and Arylboronic acids used for the reaction

Initially, while keeping the aryl diazonium salt constant (4-methoxyphenyldiazonium tetrafluoroborate), we varied the aryl boronic acid to synthesise a series of biphenyls using the improved protocol. The coupling of **1a** with unsubstituted phenylboronic acid resulted in a 91% product yield (**3a**). Substituting phenylboronic acid with 4-methylphenylboronic acid yielded the product (**3b**) with an 87% yield. However, 3-methylphenylboronic acid led to a 90% product yield (**3c**). Notably, aryl boronic acids with electron-withdrawing groups exhibited more effective conversion under the given reaction conditions. Cross-coupling products with were obtained with higher yields and shorter reaction times. For instance, **3d**, **3e**, **3f**, and **3g** were obtained with yields of 93% (50 minutes), 95% (75 minutes), 95% (55 minutes), and 88% (60 minutes), respectively. Using 4-chlorophenylboronic acid as the coupling partner of

resulted in a 90% yield (**3h**), with a reaction time of 2.5 hours observed when employing 3,4-methylenedioxyphenylboronic acid as the coupling partner of **1a**, yielding the product (**3i**) with an 85% yield. Similar results were observed when using aryl diazonium salts with methyl groups at meta- and para- positions. 3-Methylphenyldiazonium tetrafluoroborate underwent coupling with phenylboronic acid to form the product (**3q**) over 55 minutes with a yield of 91%. A slight increase in the yield was observed to 95% in 45 minutes when using 4-formylphenylboronic acid as the coupling partner, resulting in the efficient formation of product **3r**. Subsequently, changing the coupling partner to 4-acetylphenylboronic acid and 4-nitrophenylboronic acid yielded 93% of **3s** and 92% of **3t** in 55 minutes and 1 hour, respectively. Upon replacing 3-methylphenyldiazonium tetrafluoroborate with 4-methylphenyldiazonium tetrafluoroborate, the coupling reactions with 4-formylphenylboronic acid and 4-acetylphenylboronic acid resulted in good yields of the respective biphenyls (**3u** (94%) and **3v** (91%)) in 50 and 55 minutes. Following this, cross-coupling reactions were conducted using this catalytic system by taking 4-nitrophenyldiazonium tetrafluoroborate. When coupled with phenylboronic acid, the product **3k** was obtained with a yield of 90% in 50 minutes. Upon introducing an electron-donating group onto the phenylboronic acid, the yield of the coupled product decreased, while the reaction time increased. 4-Methylphenylboronic acid underwent cross-coupling with 4-nitrophenyldiazonium tetrafluoroborate to obtain 88% of the product **3l** in 50 minutes. Successively, 4-ethylphenylboronic acid yielded 86% of the product **3m** in 1 hour. The introduction of an electron-pushing tertiary butyl group at the para- position further decreased the yield of the cross-coupling product **3n** to 79% (1.5 h), while cross-coupling with 3-methoxyphenylboronic acid led to an increase in the yield to 94% in 45 minutes (**3p**). All these results have been summarised in **Table 3.2b**.

3.5.5. Reusability studies

We explored the reusability of the catalytic system under the optimised reaction conditions. The catalytic system was employed for three consecutive cycles, and a reduction in activity, resulting in a decrease in the product yield (**Table 3.3**), was observed. This decline may be attributed to the Ostwald's thermodynamic ripening, resulting to the agglomeration of nanoparticles, as evidenced by the TEM images of

the reused catalyst [18]. The heterogeneity of the system was further confirmed through the hot filtration test, where the reaction was observed to cease upon filtering the nanocatalyst from the reaction medium.

Table 3.2b. Substrate scope studies

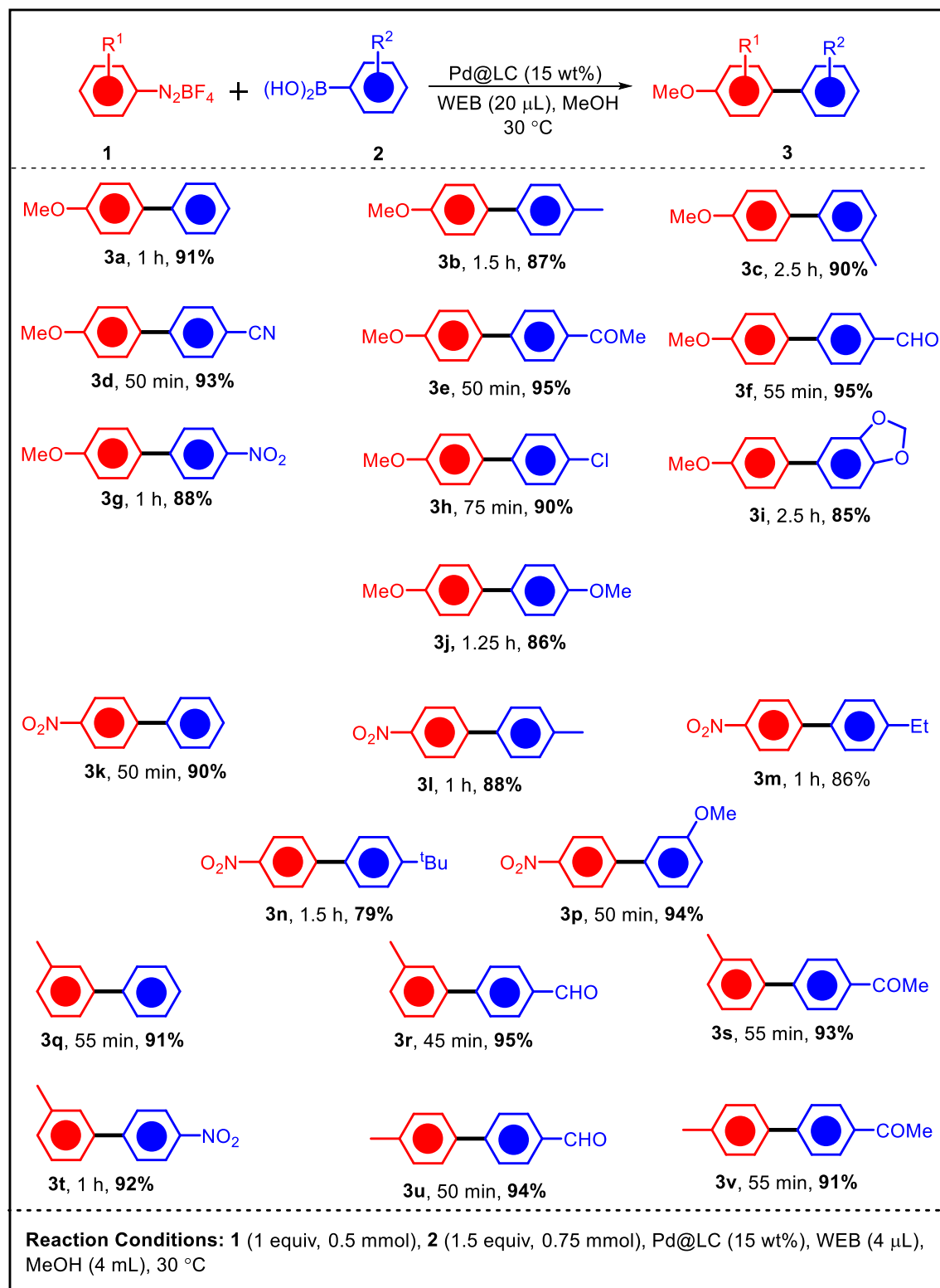
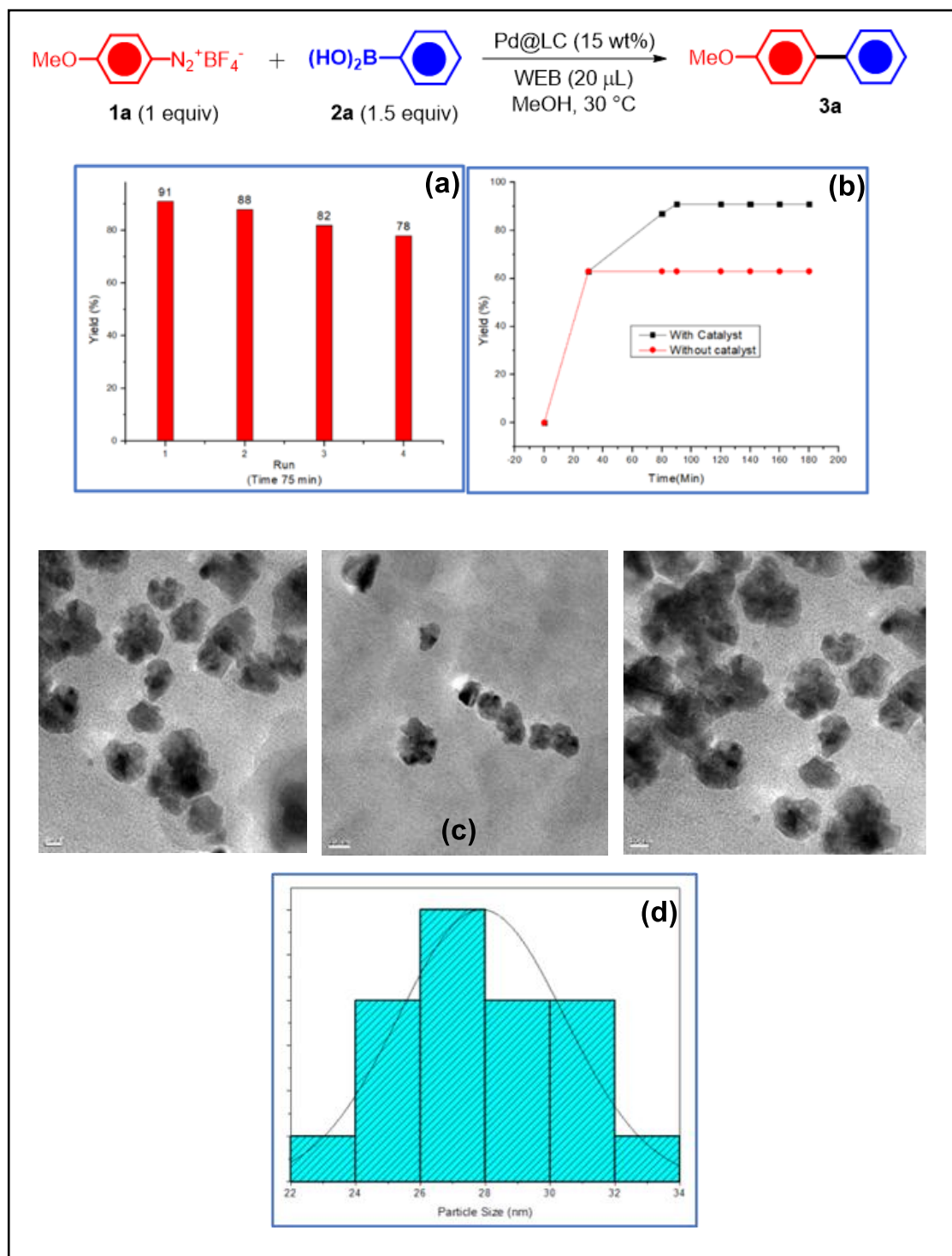


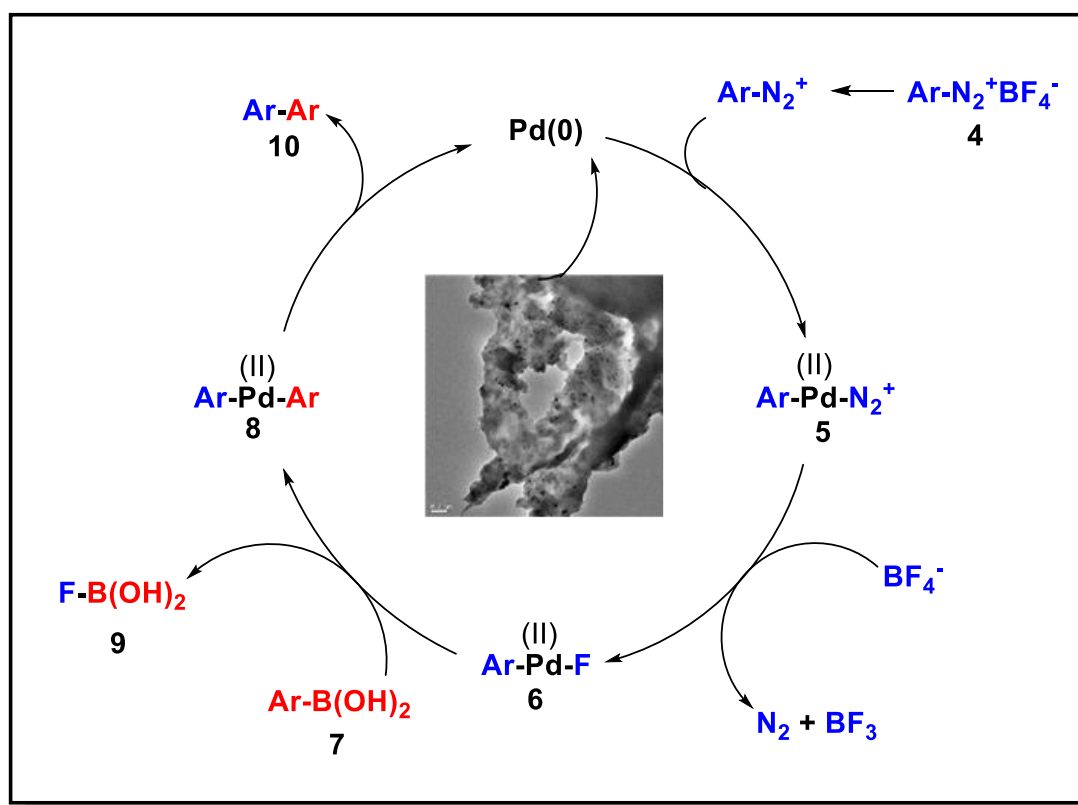
Table 3.3. a-d) TEM images of the catalyst post 3rd cycle and the corresponding reusability profile, hot filtration profile and particle size distribution



3.5.6. Plausible reaction mechanism

A plausible mechanism has been devised, and a schematic mechanistic pathway (Scheme 3.4) is elaborated below according to published literature [31]. In

this proposed mechanism, the C-N₂ bond is initially inserted into by the palladium catalyst, leading to the formation of intermediate **5**. Subsequently, the diazonium group is displaced by a fluoride ion from the tetrafluoroborate counterion, resulting in the generation of intermediate **6**. The palladium-fluoride complex **6** then interacts with arylboronic acid and undergoes transmetalation by establishing a robust F-B bond. Finally, the biaryls are formed through reductive elimination (**Scheme 3.4**).



Scheme 3.4. Plausible reaction mechanism

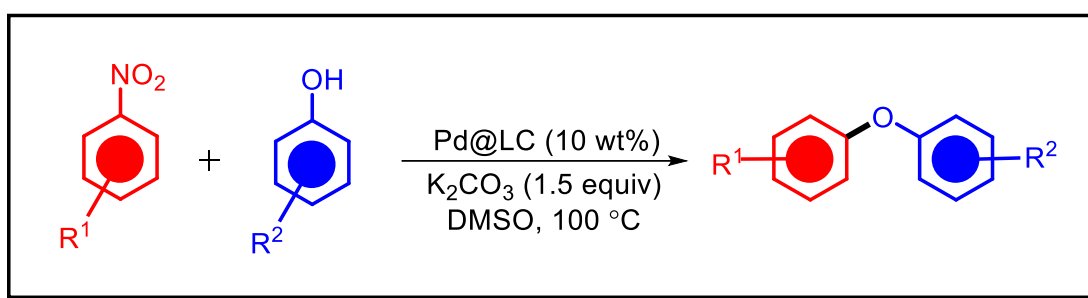
3.5.7 Conclusion

The present study demonstrates that lignocellulose derived from pomegranate peel serves as a highly adaptable and sustainable support for anchoring palladium (Pd) nanoparticles. This biomass-based support not only offers environmental advantages but also provides notable flexibility in terms of production techniques and material efficiency. Transmission Electron Microscopy (TEM) micrographs confirm the successful incorporation and uniform dispersion of Pd nanoparticles within the lignocellulose matrix, with the bio-support playing a crucial role in stabilising the nanostructures and preventing agglomeration. The resulting catalyst, referred to as Pd@LC, exhibits excellent catalytic performance in the Suzuki-Miyaura cross-

coupling reactions between arylboronic acids and aryldiazonium tetrafluoroborates, achieving good yields under mild reaction conditions. Importantly, the heterogeneous nature of the Pd@LC catalyst enables easy recovery and reuse without significant loss of activity, demonstrating its reusability over at least three consecutive reaction cycles. This underscores the potential of such green, bio-based catalytic systems in sustainable organic transformations.

Chapter 3b

Utilising Palladium (0)-Supported Lignocellulosic Biomass Catalyst for De-nitrative Cross-Coupling of Nitroarenes with Phenols



Abstract: Derived from discarded pomegranate peels, lignocellulose has been repurposed as an eco-friendly and carbon-neutral resource, serving as a foundational material for palladium nanoparticles. This transformation was achieved through a straightforward aqueous extraction method that maintained its natural structure, as evidenced by TEM analysis. The system efficiently facilitated the de-nitrative cross-coupling of aryl nitrates with phenols to form diaryl ethers.

Utilising Palladium (0)-Supported Lignocellulosic Biomass for De-nitrative Cross-coupling of Nitroarenes with Phenols

3.6. Introduction

Cross-coupling reactions involving the formation of C-O bonds have undergone a lot of developments under transition metal catalysis. First discovered in the 20th century, this class of reactions chiefly rely on palladium and copper catalysts for coupling reactions of phenols involving organo halides and boronates as coupling partners. However, significant disadvantages persist owing to the higher number of byproducts formed by the above-mentioned agents that includes homocoupling, proto dehalogenation/deboronation and *ipso*-hydroxylation [32]. As such, finding alternative cross-coupling tools for the construction of C-O bonds is important. It has been observed that electron withdrawing group activated nitroarenes can also act as efficient coupling partners with phenols, in a de-nitrative arylation for the construction of C-O bond and synthesis of diaryl ethers under transition metal catalysis [15, 16, 17]. Nitroarenes can be synthesised easily from arenes *via* aromatic nitration and can also act as starting materials and intermediates. Although readily available, however, the inertness of the C-NO₂ bond and a deactivating nature of the nitro group towards transition metal catalysis makes it hard to design such reactions. Utilising palladium as the metal core along with BrettPhos as the ligand enabled the oxidative addition of Ar-NO₂ bonds to Pd(0), making cross-couplings and ether synthesis possible [18, 19].

Diaryl ether functionality is a privileged scaffold present in several pharmaceuticals, agrochemicals, and functional materials (**Figure 3.3**). Their synthesis using nitro arenes was first reported by Chen and co-workers *via* cross-coupling with arylboronic acids under Rh (I) catalysis with aprotic polar solvents like DMF, DMSO etc [33]. This reaction was seen to involve a sequential *ipso*-hydroxylation followed by cross-coupling. Following this, Wu and team conveyed an unprecedented route for the same using much cheaper copper (II) oxide catalyst in a polar aprotic solvent under nitrogen atmosphere. An important aspect of this protocol was the complete eradication of steric effects in the formation of biaryl ether product [34]. However, this reaction suffered a major problem involving side product formation.

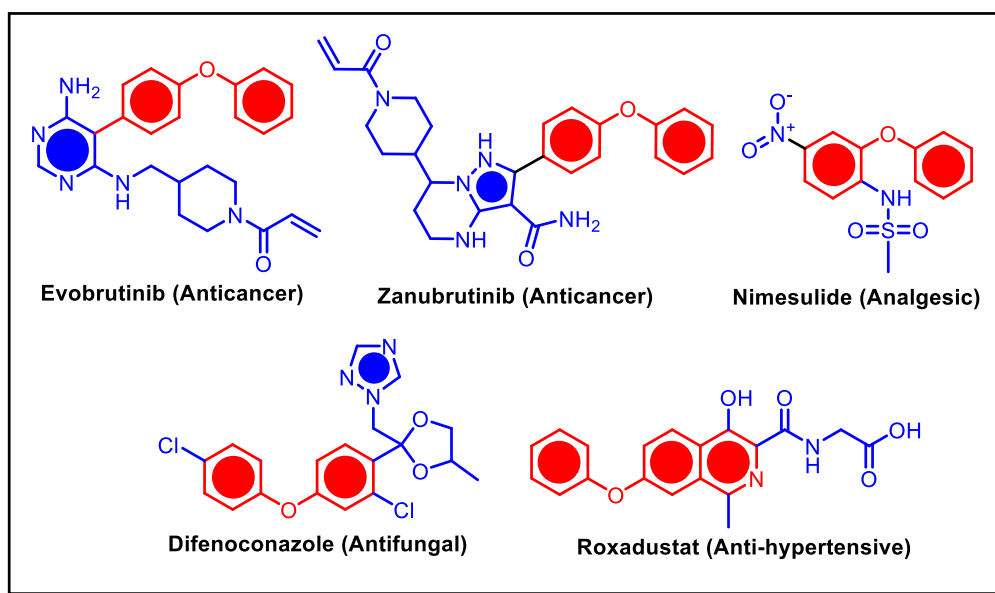
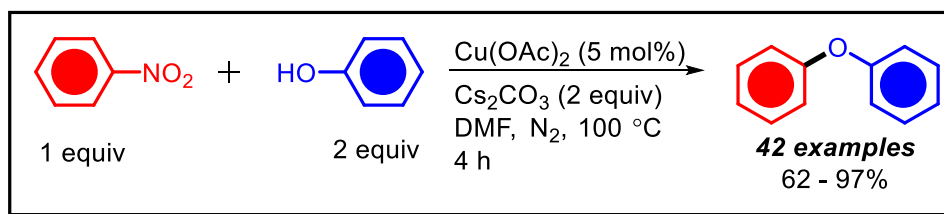


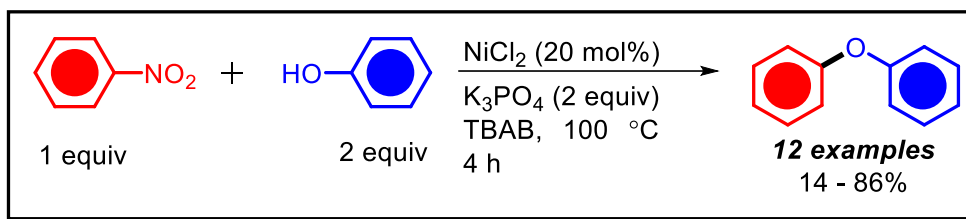
Figure 3.3. Marketed drugs based on diaryl ethers

The side reactions shown by boronic acids in this case can be removed by the utilisation of phenols instead of arylboronic acids. Chen *et al.*, first reported the *O*-arylation of phenols with nitroarenes under copper (II) catalysis. This homogeneous protocol utilises DMF as solvent with carbonate base to give *O*-arylated products under short reaction times (**Scheme 3.5**) [35].

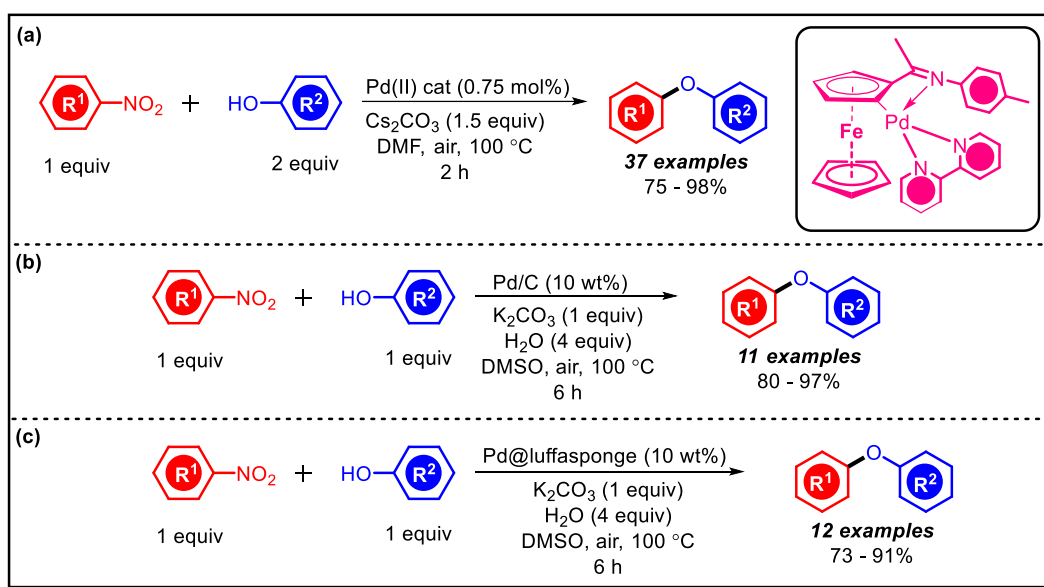


Scheme 3.5. Cu(II) catalysed cross-coupling of nitroarenes with phenols

Ghaderi and team demonstrated the same reaction under Ni(II) catalysis in the presence of potassium phosphate as base and molten TBAB as a phase transfer reagent at 100 °C. An important aspect of this reaction is the formation of alkyl ethers with the use of alcohols instead of phenols (**Scheme 3.6**) [36]. The first ever palladium catalysed protocol for the phenolic *O*-arylation using nitrobenzene was demonstrated by Wu and group. They utilised a 2,2'-bipyridyl ferrocenimine palladacycle to prepare symmetrical as well as unsymmetrical aryl ethers in modest yields.



Scheme 3.6. Ni(II) catalysed cross-coupling of nitroarenes with phenols



Scheme 3.7. Palladium catalysed *O*-arylation of phenols

A very minute catalyst loading of 0.75 mol% was seen to be enough for the transformation with of caesium carbonate base and DMF as solvent at 100 °C under air in 2 hours. The protocol was found to be well-matched with a wide range of functional groups (**Scheme 3.7(a)**) [37]. However, this protocol, requires aryl nitrates to be activated by electron withdrawing groups. Begum *et al.* reported *O*-arylation using nitroarenes this time utilising palladium on carbon (Pd/C) catalyst in the presence of potassium carbonate as base and DMF as solvent. They observed the requirement of electron withdrawing group activated nitroarenes for the reaction to take place. The group also carried out the detailed mechanistic analysis of the process which showed the reaction to be semi-heterogeneous in which the Pd(II) species leaches out into the solvent for the reaction to take place and is re-deposited as Pd(0) after the completion of the catalytic cycle (**Scheme 3.7(b)**) [38]. Recently, Thakur and co-workers reported a bio-based material that catalysed reaction of nitroarenes with phenols. They supported palladium nanoparticles over Luffa sponge as support. 10

wt% of the supported catalyst was seen to efficiently catalyse the cross-coupling of nitroarenes with phenols (**Scheme 3.7(c)**) [39]. In this chapter we study this reaction with palladium nanoparticles supported over lignocellulose derived from pomegranate peels as catalyst for de-nitrative cross-coupling.

3.7. Optimisation of the reaction conditions.

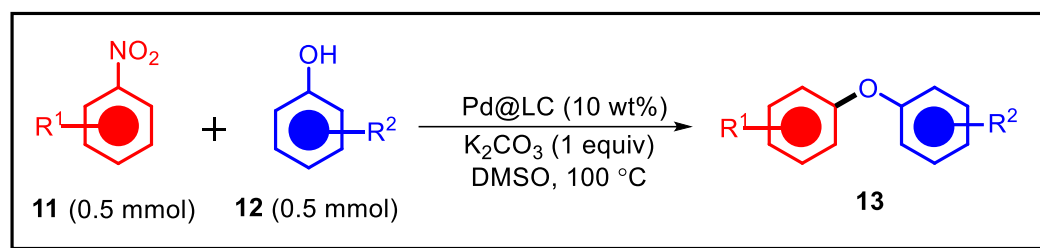
We studied the *O*-arylation of nitroarenes with phenols with Pd@LC catalyst reported in **Chapter 3a**. For this, 4-nitrobenzaldehyde and phenol were taken as model substrates. The reaction conditions were then systematically evaluated by varying the catalyst amount, base equivalents, solvent, and reaction time, while maintaining the amounts of starting materials 4a and 5a at 1 equivalent (0.5 mmol) in all cases, using DMSO (3 mL) at 100 °C (except entry 1 where temperature was maintained at 60 °C. Starting with 5 wt% of K₂CO₃ (0.5 equiv) in DMSO for 12 hours, no reaction occurred at 60 °C (**Table 3.4, Entry 1**).

However, increasing the temperature to 100 °C keeping the other parameters same for the same duration resulted in a yield of 26% (**Table 3.4, Entry 2**). Elevating the base to 1 equiv of K₂CO₃ improved the yield to 42% (**Table 3.4, Entry 3**). With 10 wt% the catalyst and K₂CO₃ (0.5 equiv), the yield rose to 62% over 12 hours (**Table 3.4, Entry 4**). When 1 equiv of K₂CO₃ was used for just 6 hours under the same conditions, the yield significantly increased to 87% (**Table 3.4, Entry 5**), and a further increase to 15 wt% catalyst with 1 equiv of K₂CO₃ yielded 87% of the product similarly (**Table 3.4, Entry 6**). Testing different solvents with 10 wt% K₂CO₃ (1 equiv) over 6 hours revealed DMAC and DMF produced yields of 63% and 59%, respectively (**Table 3.4, Entries 7 and 8**), while H₂O, MeOH, and MeOH-H₂O mixtures showed no reaction (**Table 3.4, Entries 9-11**). The use of Et₃N in the MeOH-H₂O mixture also yielded no activity (**Table 3.4, Entry 12**), whereas NaOH in DMSO produced a yield of 46% (**Table 3.4, Entry 13**). Other conditions without a catalyst or without a base resulted in no reaction (**Table 3.4, Entries 14 and 15**). These findings highlight the significant impact of catalyst concentration, base choice, and solvent on optimising yields within a defined reaction time, with consistent quantities of starting materials. The optimised reaction conditions can therefore be summarised as 4a (1 equiv, 0.5 mmol), 5a (1 equiv, 0.5 mmol), Pd@LC cat (10 wt%), K₂CO₃ (1 equiv), DMSO, 100 °C.

Table 3.4. Optimisation of the reaction conditions

<p> <chem>O=C(O)c1ccc([N+](=O)[O-])cc1</chem> + <chem>Oc1ccccc1</chem> $\xrightarrow[\text{Base, solvent, Temperature}]{\text{Pd@LC cat}}$ <chem>O=C(O)c1ccc(Oc2ccccc2)cc1</chem> </p> <p> 11a (0.5 mmol) 12a (0.5 mmol) 13a </p>					
Entry	Catalyst amount (wt%)	Base (equiv)	Solvent	Time	Yield (%)
1	5	K ₂ CO ₃ (0.5)	DMSO	12 h	NR ^b
2	5	K ₂ CO ₃ (0.5)	DMSO	12 h	26
3	5	K ₂ CO ₃ (1)	DMSO	12 h	42
4	10	K ₂ CO ₃ (0.5)	DMSO	12 h	62
5	10	K₂CO₃ (1)	DMSO	6 h	85
6	15	K ₂ CO ₃ (1)	DMSO	6 h	87
7	10	K ₂ CO ₃ (1)	DMAC	6 h	63
8	10	K ₂ CO ₃ (1)	DMF	6 h	59
9	10	K ₂ CO ₃ (1)	H ₂ O	6 h	NR
10	10	K ₂ CO ₃ (1)	MeOH	6 h	NR
11	10	K ₂ CO ₃ (1)	MeOH-H ₂ O	6 h	NR
12	10	Et ₃ N (1)	MeOH-H ₂ O	6 h	NR
13	10	NaOH (1)	DMSO	6 h	46
14	-	K ₂ CO ₃ (1)	DMSO	6 h	NR
15	10	-	DMSO	6 h	NR
Reaction conditions: 11a (1 equiv, 0.5 mmol), 12a (1 equiv, 0.5 mmol), ^b Temperature: 60 °C (100 °C in all other entries)					

3.8. General procedure for the *O*-arylation reaction



Scheme 3.8. General procedure for *O*-arylation

A thoroughly washed and dried round bottom flask was charged with 1 equivalent (0.5 mmol) of the nitroarene and 1 equivalent (0.5 mmol) of the phenol. This was followed by the addition of 3 mL of the solvent, DMSO followed by stirring for 5 minutes at room temperature so that the reactants dissolve. The temperature was then increased to 100 °C. Subsequently, 10 wt% of the catalyst and 1 equivalent of the base were added and the reaction and the reaction mixture were connected to a reflux condenser and the reaction mixture was allowed to stir for 6 hours (monitored *via* TLC). After the completion of the reaction, the reaction mixture was poured to ice water and extracted with Ethyl acetate-water system. The combined organic layers were then dried with anhydrous sodium sulfate and dried under vacuum to obtain the crude product. The crude product was purified using 1% Ethylacetate in Hexane to obtain the pure product (**Scheme 3.8**).

3.9. Substrate scope studies

After establishing the optimal conditions, the substrate scope of the reaction as illustrated in **Table 3.5** was studied. The reaction proceeded successfully with activated nitroarenes bearing electron-withdrawing groups only. All reactions were completed within 6 hours, yielding various products that demonstrated the efficiency of diverse coupling partners. For example, product **13a**, formed from 4-nitrobenzaldehyde and phenol, produced phenyl-4-formylphenyl ether with an impressive 87% yield. Similarly, product **13b**, from 4-nitrobenzaldehyde and 4-chlorophenol, yielded 4-chloro-4'-formyldiphenyl ether at 83%. The reaction between 4-nitrobenzaldehyde and 4-methoxyphenol yielded product **13c**, 4-formyl-4'-methoxydiphenyl ether, at 76%. Product **13d**, derived from 4-nitrobenzaldehyde and 4-tertiary butylphenol, achieved 80% yield for 4-formyl-4'-tertiary butyldiphenyl

ether. Additional successful reactions included 4-cyanonitrobenzene with phenol, yielding product **13e** (4-cyanodiphenyl ether, 82%), and 4-cyanonitrobenzene with 4-chlorophenol, producing product **13f** (4-chloro-4'-cyanodiphenyl ether, 78%). Product **13g**, formed from 4-chloronitrobenzene and phenol, gave 4-chlorodiphenyl ether at 77%. The reaction between 4-nitrobenzaldehyde and 2-naphthol produced product **13h** (4-formylphenoxy-2-naphthalene) with a 73% yield. However, product **13i**, resulting from 4-chloronitrobenzene and 4-chlorophenol, yielded 71%, and attempts to produce product **13j** from 4-methylnitrobenzene and 4-methoxyphenol were unsuccessful. Similarly, Product **13k**, from 4-methylnitrobenzene and 4-nitrophenol, was not obtained. The previous protocols for this reaction that includes the works of Begum *et al.*, and Kakaty *et al.*, also show the failure of the reaction in presence of electron donating groups on the aromatic nucleus of the nitroarene [f, g]. Theoretical studies suggest the oxidative addition of the nitroarene to the Pd(0) center to take place *via* electron transfer from Pd(0) to the antibonding LUMO of the nitroarene which is more feasible in case of activated nitroarenes which possess a lower energy LUMO unlike that of nitroarenes with electron donating groups that possess a LUMO of much higher energy.

3.10. Heterogeneity studies

The Pd@LC catalyst was checked for heterogeneity under the given reaction conditions. The optimised reaction when subjected to hot filtration test showed the progression of the reaction after hot filtration. This shows the leaching of palladium species during the reaction [40] (**Figure 3.4**).

3.11. Reaction mechanism

The mechanistic path for this kind of cross-coupling of nitroarenes and phenols was comprehensively studied by Bora and co-workers. The oxidative addition of nitroarenes to the Pd surface promotes their conversion, forming ArPd(II)NO_2 species in solution. This intermediate ultimately produces the desired product while regenerating free Pd(0) to restart the catalytic cycle, as illustrated in **Scheme 3.9**.

Table 3.5. Substrate scope studies

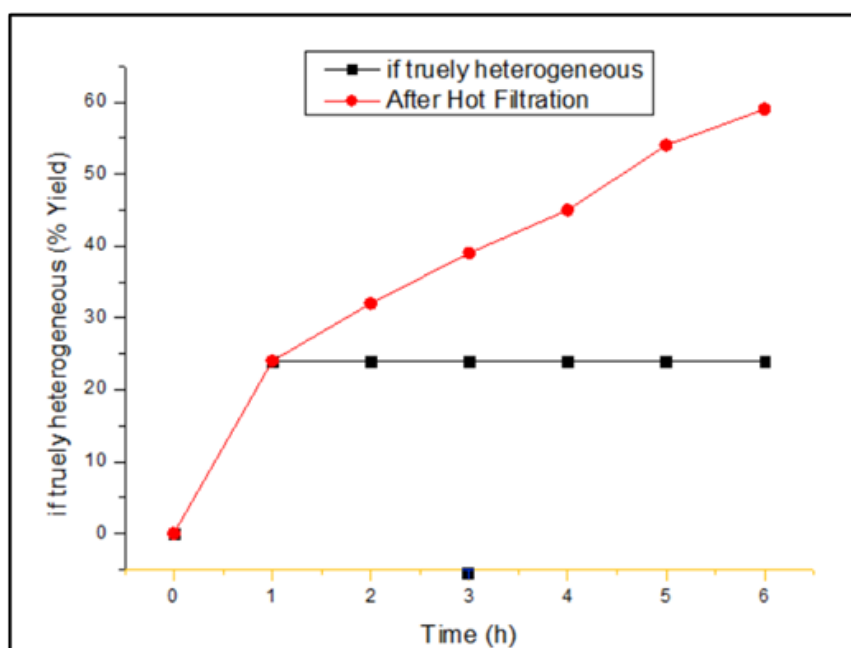
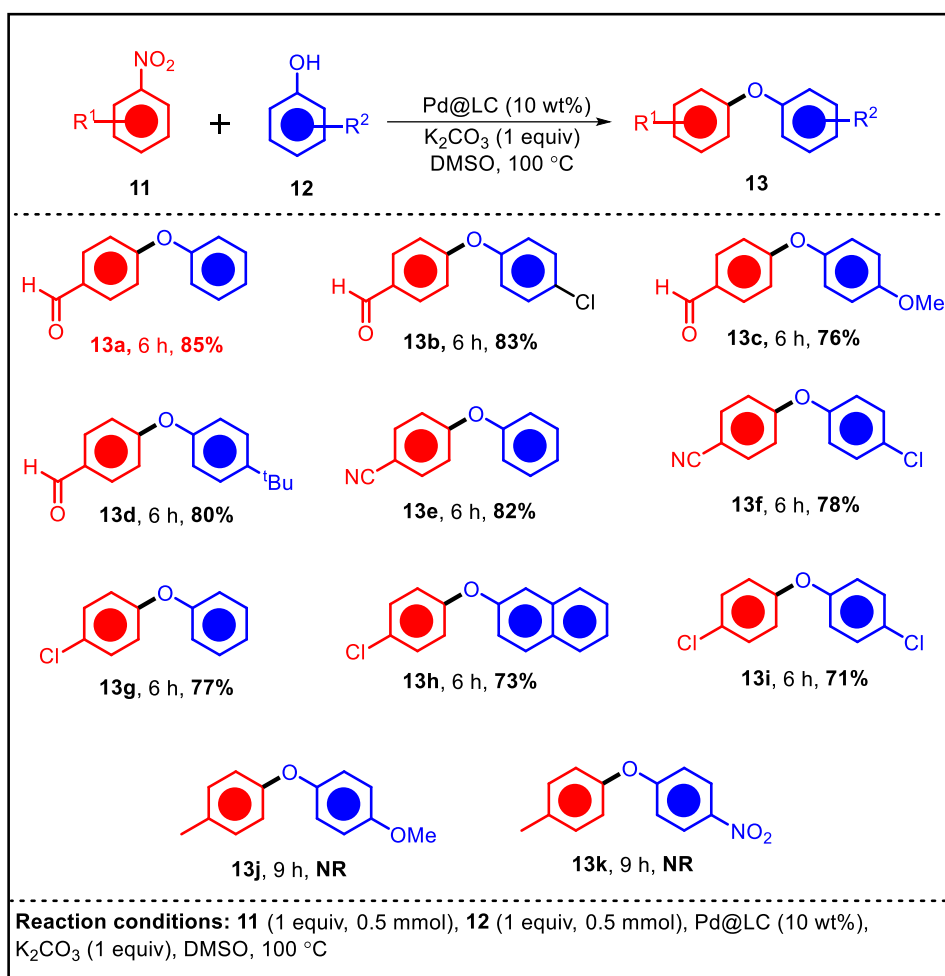
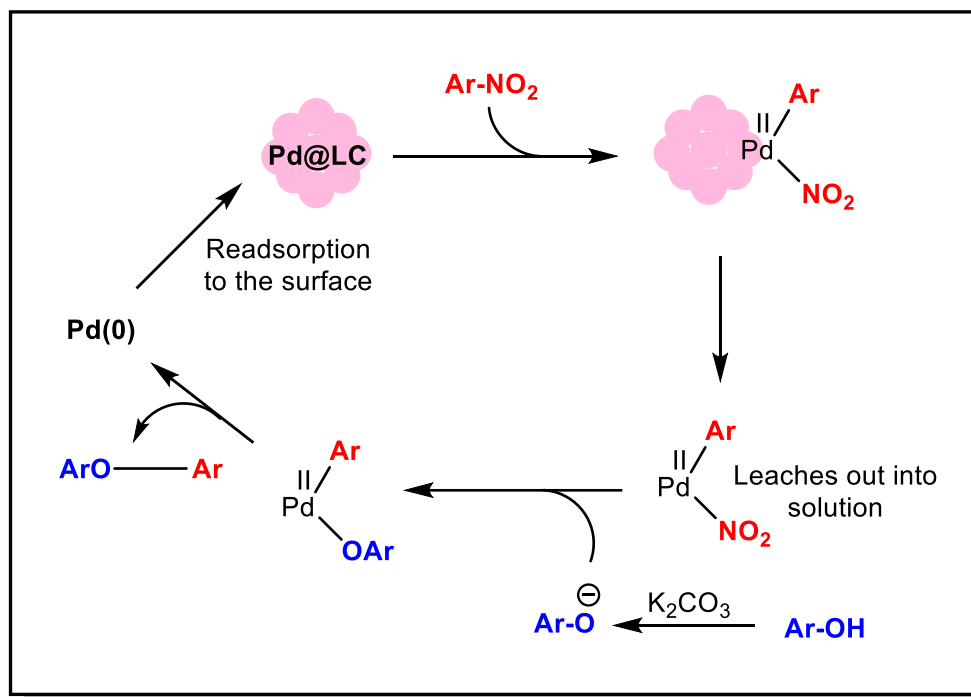


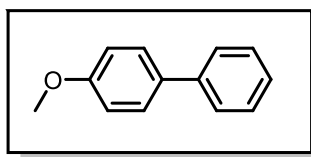
Figure 3.4. Hot filtration profile



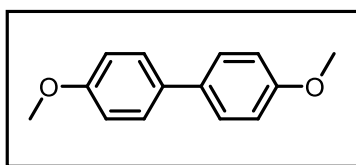
Scheme 3.9. Reaction mechanism for *O*-arylation

3.12. Conclusion

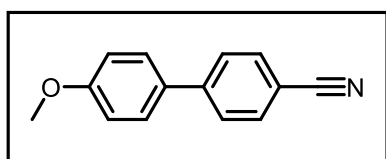
The palladium nanocatalyst supported over lignocellulose derived from pomegranate peels shows good catalytic activity in the *O*-arylation of phenols using nitroarenes. The reaction requires electron withdrawing group activated nitroarenes and proceeds *via* the leaching of the Pd(II) species post oxidative addition.

3.13. ^1H and ^{13}C NMR Data

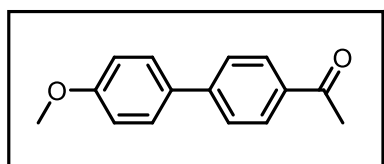
3a. 4-Methoxybiphenyl, white solid, m.p. 87 – 88 °C, ^1H NMR (600 MHz, CHLOROFORM-D) δ (ppm) 7.60 – 7.57 (m, 2H), 7.56 (d, J = 8.7 Hz, 2H), 7.46 – 7.44 (m, 2H), 7.35 – 7.32 (m, 1H), 7.01 (d, J = 8.7 Hz, 2H), 3.88 (s, 3H). ^{13}C NMR (150 MHz, CHLOROFORM-D) δ (ppm) 159.1, 140.8, 133.8, 128.7, 128.2, 126.8, 126.7, 114.2, 55.4.



3b. 4,4'-Dimethoxybiphenyl, white solid, m.p. 180 °C, ^1H NMR (600 MHz, CHLOROFORM-D) δ (ppm) 7.50 (d, J = 8.8 Hz, 4H), 6.98 (d, J = 8.8 Hz, 4H), 3.87 (s, 6H). ^{13}C NMR (150 MHz, CHLOROFORM-D) δ (ppm) 158.7, 133.5, 127.8, 114.2, 55.4.

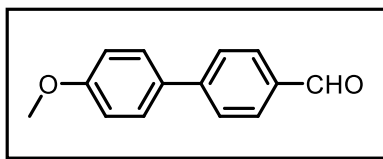


3d. 4'-Methoxy-[1,1'-biphenyl]-4-carbonitrile, white solid, ^1H NMR (600 MHz, CHLOROFORM-D) δ (ppm) 7.71 (d, J = 8.5 Hz, 2H), 7.66 (d, J = 8.5 Hz, 2H), 7.56 (d, J = 8.8 Hz, 2H), 7.03 (d, J = 8.8 Hz, 2H), 3.89 (s, 3H). ^{13}C NMR (150 MHz, CHLOROFORM-D) δ (ppm) 160.2, 145.2, 132.6, 131.5, 128.4, 127.1, 119.1, 114.5, 110.1, 55.4.

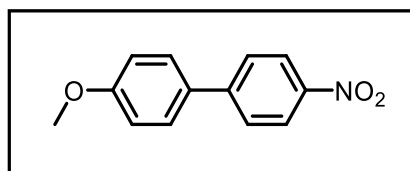


3e. 1-(4'-Methoxy-[1,1'-biphenyl]-4-yl)ethan-1-one, white solid, ^1H NMR (600 MHz, CHLOROFORM-D) δ (ppm) 8.03 (d, J = 8.3 Hz, 2H), 7.67 (d, J = 8.3 Hz, 2H), 7.60 (d, J = 8.7 Hz, 2H), 7.02 (d, J = 8.7 Hz, 2H), 3.88 (s, 3H), 2.65 (s, 3H). ^{13}C NMR (150 MHz,

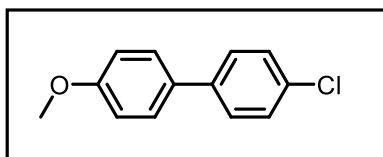
CHLOROFORM-D) δ (ppm) 197.8, 159.9, 145.4, 135.3, 132.2, 129.0, 128.4, 126.6, 114.4, 55.4, 26.7.



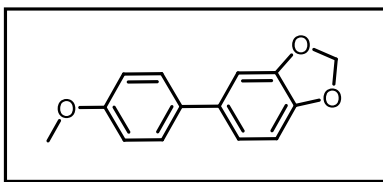
3f. 4'-Methoxy-[1,1'-biphenyl]-4-carbaldehyde, white solid, ^1H NMR (600 MHz, CHLOROFORM-D) δ (ppm) 10.05 (s, 1H), 7.95 (d, J = 8.3 Hz, 2H), 7.74 (d, J = 8.2 Hz, 2H), 7.62 (d, J = 8.8 Hz, 2H), 7.03 (d, J = 8.8 Hz, 2H), 3.89 (s, 3H). ^{13}C NMR (150 MHz, CHLOROFORM-D) δ (ppm) 191.9, 160.1, 146.8, 134.7, 132.0, 130.3, 128.5, 127.1, 114.5, 55.4.



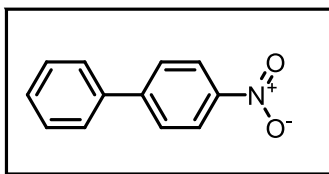
3g. 4-Methoxy-4'-nitro-1,1'-biphenyl, white solid. ^1H NMR (600 MHz, CHLOROFORM-D) δ (ppm) 7.50 (d, J = 8.8 Hz, 4H), 6.98 (d, J = 8.8 Hz, 4H), 3.87 (s, 3H). ^{13}C NMR (150 MHz, CHLOROFORM-D) δ (ppm) 159.4, 148.2, 144.9, 131.2, 129.1, 128.7, 124.5, 114.7, 56.0.



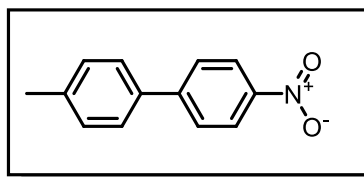
3h. 4-Chloro-4'-methoxy-1,1'-biphenyl, white solid, ^1H NMR (600 MHz, CHLOROFORM-D) δ (ppm) 7.52 (d, J = 8.8 Hz, 2H), 7.50 (d, J = 8.7 Hz, 2H), 7.41 (d, J = 8.7 Hz, 2H), 7.00 (d, J = 8.8 Hz, 2H), 3.88 (s, 3H). ^{13}C NMR (150 MHz, CHLOROFORM-D) δ (ppm) 159.4, 139.3, 132.7, 132.5, 128.9, 128.0, 127.9, 114.3, 55.4.



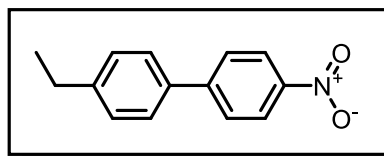
3j. 5-(4-Methoxyphenyl)benzo[d][1,3]dioxole, white solid, ^1H NMR (600 MHz, CHLOROFORM-D) δ (ppm) 7.47 (d, J = 8.8 Hz, 2H), 7.06 – 6.98 (m, 2H), 6.97 (d, J = 8.8 Hz, 2H), 6.88 (m, 1H), 6.01 (s, 2H), 3.87 (s, 3H). ^{13}C NMR (150 MHz, CHLOROFORM-D) δ (ppm) 158.9, 148.0, 146.6, 135.3, 133.6, 127.9, 120.3, 114.2, 108.5, 107.5, 101.1, 55.4.



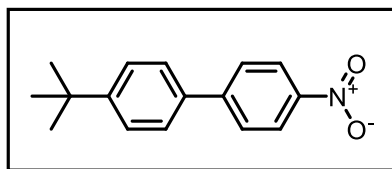
3k. 4-Nitro-1,1'-biphenyl, pale yellow solid, ^1H NMR (600 MHz, CHLOROFORM-D) δ (ppm) 8.32 (d, J = 8.8 Hz, 2H), 7.76 (d, J = 8.8 Hz, 2H), 7.65 (m, 2H), 7.53 (m, 2H), 7.49 – 7.45 (m, 1H). ^{13}C NMR (150 MHz, CHLOROFORM-D) δ (ppm) 147.6, 147.1, 138.8, 129.2, 128.9, 127.8, 127.4, 124.0.



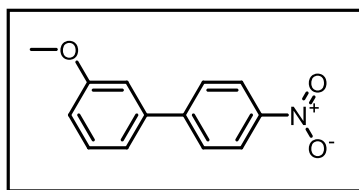
3l. 4-Methyl-4'-nitro-1,1'-biphenyl, white solid, ^1H NMR (600 MHz, CHLOROFORM-D) δ (ppm) 8.30 (d, J = 8.8 Hz, 2H), 7.74 (d, J = 8.8 Hz, 2H), 7.55 (d, J = 8.0 Hz, 2H), 7.33 (d, J = 8.0 Hz, 2H), 2.45 (s, 3H). ^{13}C NMR (150 MHz, CHLOROFORM-D) δ (ppm) 147.6, 146.8, 139.1, 135.8, 129.9, 127.5, 127.2, 124.1, 21.2.



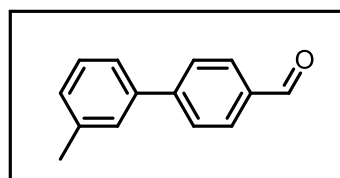
3m. 4-Ethyl-4'-nitro-1,1'-biphenyl, pale yellow solid, ^1H NMR (600 MHz, CHLOROFORM-D) δ (ppm) 8.31 (d, J = 8.8 Hz, 2H), 7.75 (d, J = 8.8 Hz, 2H), 7.58 (d, J = 8.2 Hz, 2H), 7.36 (d, J = 8.2 Hz, 2H), 2.75 (q, J = 7.6 Hz, 2H), 1.31 (t, J = 7.6 Hz, 3H). ^{13}C NMR (150 MHz, CHLOROFORM-D) δ (ppm) 147.6, 146.8, 145.4, 136.1, 128.7, 127.5, 127.3, 124.1, 28.6, 15.5.



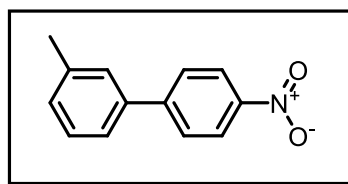
3n. 4-(tert-Butyl)-4'-nitro-1,1'-biphenyl, white solid, ^1H NMR (600 MHz, CDCl_3) δ (ppm) 8.31 (d, $J = 8.9$ Hz, 2H), 7.76 (d, $J = 8.9$ Hz, 2H), 7.61 (d, $J = 8.5$ Hz, 2H), 7.56 (d, $J = 8.6$ Hz, 2H), 1.41 (s, 9H). ^{13}C NMR (150 MHz, CDCl_3) δ (ppm) 152.3, 147.5, 146.9, 135.8, 127.5, 127.1, 126.2, 124.1, 34.7, 31.3.



3p. 3-methoxy-4'-nitro-1,1'-biphenyl, white solid, ^1H NMR (600 MHz, CHLOROFORM-D) δ (ppm) 8.30 (d, $J = 8.8$ Hz, 2H), 7.74 (d, $J = 8.8$ Hz, 2H), 7.43 (t, $J = 7.9$ Hz, 1H), 7.22 (m, 1H), 7.17 – 7.14 (m, 1H), 7.03 – 6.99 (m, 1H), 3.90 (s, 3H). ^{13}C NMR (150 MHz, CHLOROFORM-D) δ (ppm) 160.2, 147.5, 147.1, 140.2, 130.2, 127.9, 124.1, 119.8, 114.1, 113.3, 55.4.

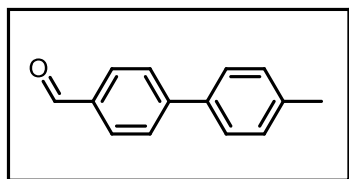


3r. 3-Methyl-4'-formylbiphenyl, white solid, ^1H NMR (600 MHz, CHLOROFORM-D) δ (ppm) 10.08 (s, 1H), 7.97 (d, $J = 8.2$ Hz, 2H), 7.77 (d, $J = 8.2$ Hz, 2H), 7.50 – 7.37 (m, 3H), 7.24-7.27 (m, 1H), 2.46 (s, 3H). ^{13}C NMR (150 MHz, CHLOROFORM-D) δ (ppm) 192.0, 147.4, 139.7, 138.7, 135.1, 130.2, 129.2, 128.9, 128.1, 127.7, 124.5, 21.5.

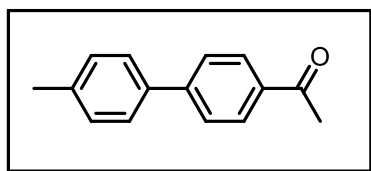


3t. 3-Methyl-4'-nitro-1,1'-biphenyl, white solid, ^1H NMR (600 MHz, CHLOROFORM-D) δ (ppm) 8.31 (d, $J = 8.7$ Hz, 2H), 7.52 (d, $J = 8.7$ Hz, 2H), 7.39 – 7.29 (m, 3H), 7.24 (d,

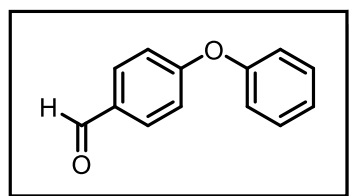
$J = 7.5$ Hz, 1H), 2.30 (s, 3H). ^{13}C NMR (150 MHz, CHLOROFORM-D) δ (ppm) 148.8, 146.8, 139.6, 135.1, 130.7, 130.1, 129.4, 128.5, 126.1, 123.4, 20.4.



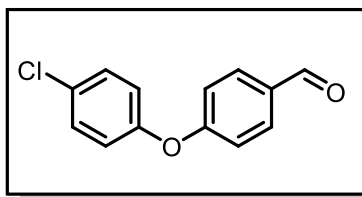
3u. 4'-Methyl-[1,1'-biphenyl]-4-carbaldehyde, white solid, ^1H NMR (600 MHz, CHLOROFORM-D) δ (ppm) 10.07 (s, 1H), 7.96 (d, $J = 8.2$ Hz, 2H), 7.77 (d, $J = 8.2$ Hz, 2H), 7.57 (d, $J = 8.1$ Hz, 2H), 7.32 (d, $J = 8.1$ Hz, 2H), 2.44 (s, 3H). ^{13}C NMR (150 MHz, CHLOROFORM-D) δ (ppm) 192.0, 147.2, 138.5, 136.8, 135.0, 130.3, 129.8, 127.4, 127.2, 21.2.



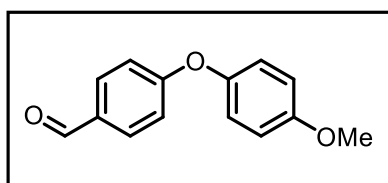
3v. 1-(4'-Methyl-[1,1'-biphenyl]-4-yl)ethan-1-one, white solid, ^1H NMR (600 MHz, CHLOROFORM-D) δ (ppm) 8.04 (d, $J = 8.4$ Hz, 2H), 7.70 (d, $J = 8.4$ Hz, 2H), 7.56 (d, $J = 8.1$ Hz, 2H), 7.30 (d, $J = 8.1$ Hz, 2H), 2.66 (s, 3H), 2.43 (s, 3H). ^{13}C NMR (150 MHz, CHLOROFORM-D) δ (ppm) 197.8, 145.7, 138.3, 137.0, 135.6, 129.7, 128.9, 127.1, 127.0, 26.7, 21.2.



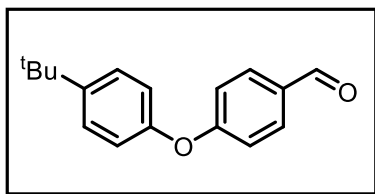
13a. 4-phenoxybenzaldehyde: ^1H NMR (400 MHz, CHLOROFORM-D) δ (ppm) δ 9.91 (s, 1H), 7.83 (d, $J = 8.9$ Hz, 2H), 7.41 (t, $J = 8$ Hz, 2H), 7.22 (t, $J = 7.4$ Hz, 1H), 7.06 (dd, $J = 11.0, 8.1$ Hz, 4H). NMR (100 MHz) δ (ppm) 190.9, 163.3, 155.2, 132.1, 131.3, 130.3, 125, 120.5, 117.6.



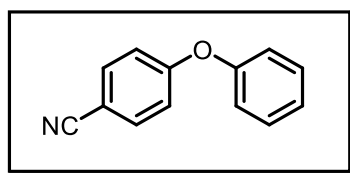
13b. 4-(4-chlorophenoxy)benzaldehyde: ^1H NMR (400 MHz, CHLOROFORM-D) δ (ppm) 9.92 (s, 1H), 7.84 (d, J = 8.8 Hz, 2H), 7.36 (d, J = 9.0 Hz, 2H), 7.04 (d, J = 8.8 Hz, 2H), 7.01 (d, J = 9.0 Hz, 2H), ^{13}C NMR (100 MHz, CHLOROFORM-D) δ (ppm) 190.8, 162.8, 153.8, 132.1, 131.6, 130.3, 130.2, 121.8, 117.7.



13c. 4'-methoxy-[1,1'-biphenyl]-4-carbaldehyde: ^1H NMR (400 MHz, CHLOROFORM-D) δ (ppm) 9.89 (s, 1H), 7.81 (d, J = 8.8 Hz, 2H), 7.02 (d, J = 9.2 Hz, 2H), 6.99 (d, J = 8.8 Hz, 2H), 6.92 (d, J = 9.2 Hz, 2H), 3.82 (s, 3H). NMR (100 MHz, CHLOROFORM-D) δ (ppm) 190.8, 164.2, 157.0, 148.2, 132.0, 131.0, 121.9, 116.8, 115.2, 55.7.

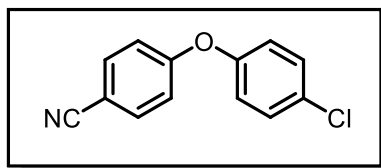


13d. 4-(4-(tert-butyl)phenoxy)benzaldehyde: ^1H NMR (400 MHz, CHLOROFORM-D) δ (ppm) 9.90 (s, 1H), 7.82 (d, J = 8.8 Hz, 2H), 7.40 (d, J = 8.8 Hz, 2H), 7.04 (d, J = 8.6 Hz, 2H), 7.00 (d, J = 8.6 Hz, 2H), 1.33 (s, 9H). ^{13}C NMR (100 MHz, CHLOROFORM-D) δ (ppm) 190.9, 163.7, 152.6, 148.1, 132.0, 131.1, 127.1, 120.0, 117.4, 34.6, 31.6.



13e. 4-Cyanophenoxybenzaldehyde: ^1H NMR (400 MHz, CHLOROFORM-D) δ (ppm) 7.58 (d, J = 9.0 Hz, 2H), 7.45 – 7.35 (m, 2H), 7.22 (m, 1H), 7.09 – 7.03 (m, 2H), 6.99 (d,

$J = 9.0$ Hz, 2H). ^{13}C NMR (100 MHz, CHLOROFORM-D) δ (ppm) 161.8, 154.9, 134.2, 130.3, 125.3, 120.5, 119.0, 118.0, 105.9.



13f. 4-(4-chlorophenoxy)benzonitrile: ^1H NMR (400 MHz, CHLOROFORM-D) δ (ppm) 8.19 (d, $J = 9.4$ Hz, 2H), 7.38 (d, $J = 9.1$ Hz, 2H), 7.02 (d, $J = 9.1$ Hz, 2H), 7.00 (d, $J = 9.4$ Hz, 2H). ^{13}C NMR (100 MHz) δ (ppm) 163.0, 153.4, 143.0, 130.8, 130.5, 130.4, 126.1, 121.9, 117.3.

3.14. Representative NMR Spectra

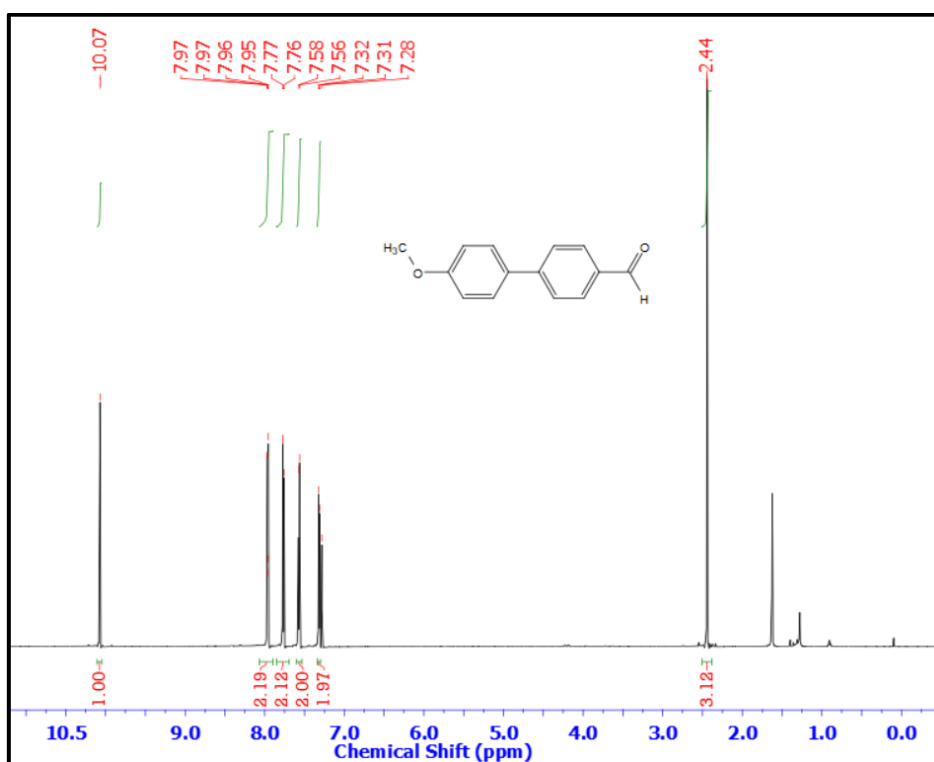


Figure 3.5. ¹H NMR Spectrum of 3c (4'-methoxy-[1,1'-biphenyl]-4-carbaldehyde) in CDCl₃

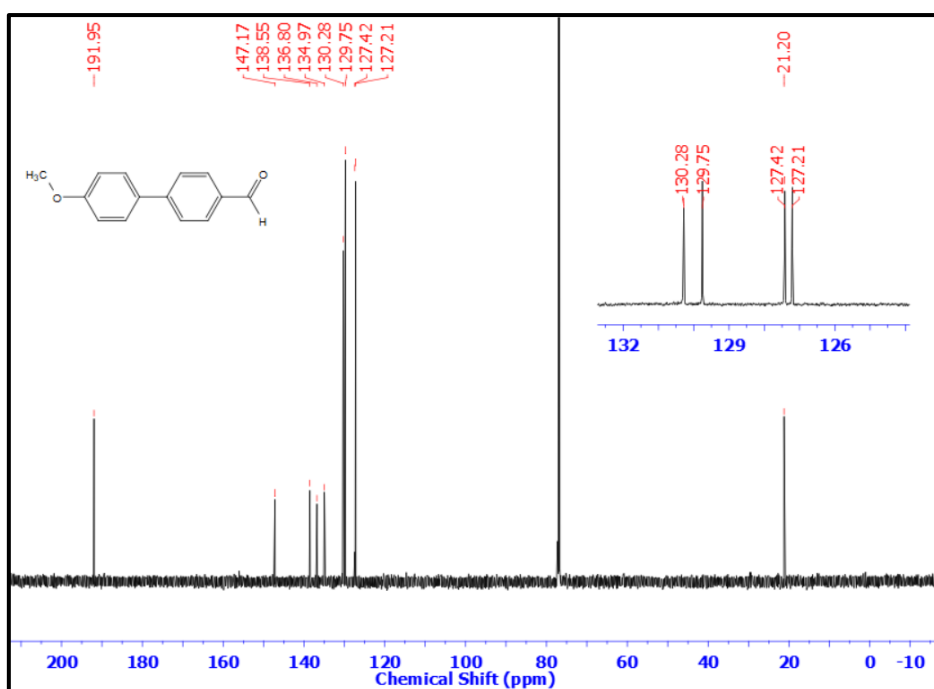


Figure 3.6. ¹³C NMR Spectrum of 3c (4'-methoxy-[1,1'-biphenyl]-4-carbaldehyde) in CDCl₃

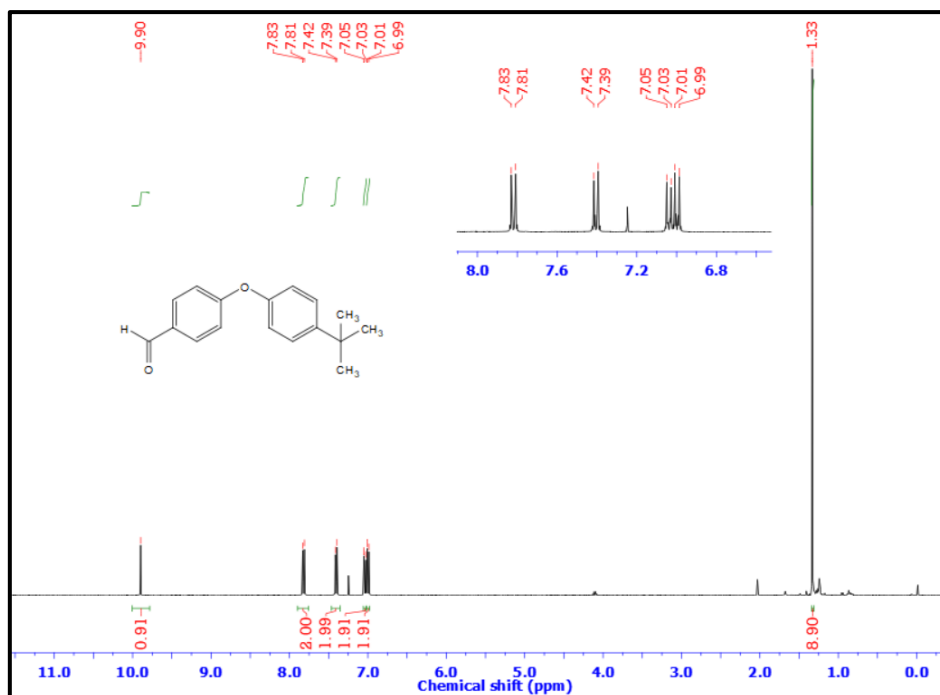


Figure 3.7. ^1H NMR Spectrum of 13d (4-(4-(*tert*-Butyl)phenoxy)benzaldehyde) in CDCl_3

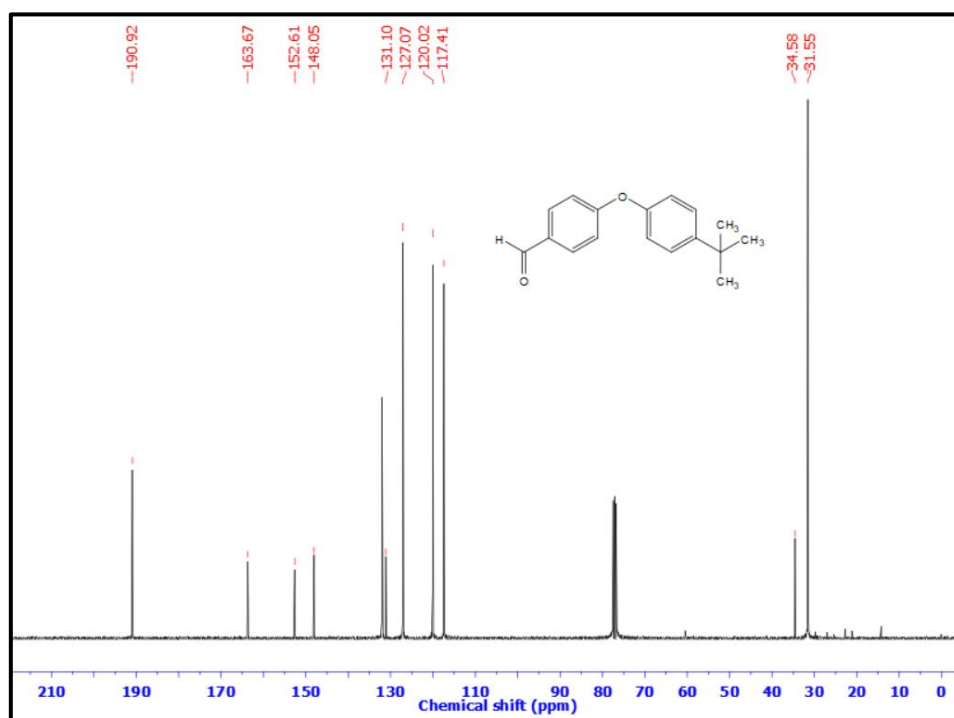


Figure 3.8. ^{13}C NMR Spectrum of 13d (4-(4-(*tert*-Butyl)phenoxy)benzaldehyde) in CDCl_3

3.15. Bibliography

- [1] Ruiz-Castillo, P. and Buchwald, S. L. Applications of palladium-catalysed C–N cross-coupling reactions. *Chemical Reviews*, 116(19):12564-12649, 2016.
- [2] Johansson Seechurn, C. C., Kitching, M. O., Colacot, T. J., and Snieckus, V. Palladium-catalysed cross-coupling: a historical contextual perspective to the 2010 Nobel Prize. *Angewandte Chemie International Edition*, 51(21):5062-5085, 2012.
- [3] Campeau, L.-C. and Hazari, N. Cross-coupling and related reactions: connecting past success to the development of new reactions for the future. *Organometallics*, 38(1):3-35, 2018.
- [4] Yasuda, N. Application of cross-coupling reactions in Merck. *Journal of Organometallic Chemistry*, 653(1-2):279-287, 2002.
- [5] Vijayan, A., Rao, D.N., Radhakrishnan, K.V., Lam, P.Y. and Das, P. Advances in carbon–element bond construction under Chan–Lam cross-coupling conditions: a second decade. *Synthesis*, 53(05):805-847, 2021.
- [6] a) Han, F.-S. Transition-metal-catalysed Suzuki–Miyaura cross-coupling reactions: a remarkable advance from palladium to nickel catalysts. *Chemical Society Reviews*, 42(12):5270-5298, 2013; b) Roughley, S.D. and Jordan, A.M., 2011. The medicinal chemist's toolbox: an analysis of reactions used in the pursuit of drug candidates. *Journal of Medicinal Chemistry*, 54(10):3451-3479, 2011.
- [7] Trzeciak, A. and Augustyniak, A. The role of palladium nanoparticles in catalytic C–C cross-coupling reactions. *Coordination Chemistry Reviews*, 384:1-20, 2019.
- [8] Zhu, Y., Dong, W., and Tang, W. Palladium-catalysed cross-couplings in the synthesis of agrochemicals. *Advanced Agrochem*, 2022.
- [9] Devendar, P., Qu, R.-Y., Kang, W.-M., He, B., and Yang, G.-F. Palladiumcatalysed cross-coupling reactions: a powerful tool for the synthesis of agrochemicals. *Journal of Agricultural and Food Chemistry*, 66(34):8914- 8934, 2018.
- [10] So, C. M. and Kwong, F. Y. Palladium-catalysed cross-coupling reactions of aryl mesylates. *Chemical Society Reviews*, 40(10):4963-4972, 2011.

- [11] Yin, L. and Liebscher, J. Carbon– carbon coupling reactions catalysed by heterogeneous palladium catalysts. *Chemical Reviews*, 107(1):133-173, 2007.
- [12] Beletskaya, I.P., Alonso, F. and Tyurin, V. The Suzuki-Miyaura reaction after the Nobel prize. *Coordination Chemistry Reviews*, 385: 137-173, 2019.
- [13] Vásquez-Céspedes, S., Betori, R.C., Cismesia, M.A., Kirsch, J.K. and Yang, Q. Heterogeneous catalysis for cross-coupling reactions: an underutilised powerful and sustainable tool in the fine chemical industry? *Organic Process Research & Development*, 25(4):740-753, 2021.
- [14] a) Kashiwara, M. and Nakao, Y. Cross-coupling reactions of nitroarenes. *Accounts of chemical research*, 54(14):2928-2935, 2021; b) Muto, K., Okita, T. and Yamaguchi, J. Transition-metal-catalysed de-nitrative coupling of nitroarenes. *ACS Catalysis*, 10(17):9856-9871, 2020. c) Cai, X.H., Zhang, H. and Guo, H. De-nitrative coupling reaction: A powerful synthetic tool in functional transformation. *Current Organic Chemistry*, 23(10):1131-1150, 2019.
- [15] Yadav, M.R., Nagaoka, M., Kashiwara, M., Zhong, R.L., Miyazaki, T., Sakaki, S. and Nakao, Y. The Suzuki–Miyaura coupling of nitroarenes. *Journal of the American Chemical Society*, 139(28):9423-9426, 2017.
- [16] Feng, B., Yang, Y., and You, J. A methylation platform of unconventional inert aryl electrophiles: trimethylboroxine as a universal methylating reagent. *Chemical Science*, 11(23):6031-6035, 2020.
- [17] Kashiwara, M., Inoue, F., Yadav, M. R., and Nakao, Y. Buchwald–Hartwig amination of nitroarenes. *Angewandte Chemie International Edition*, 56(43):13307-13309, 2017.
- [18] Yang, Y., Feng, B., and You, J. Palladium-catalysed de-nitrative Sonogashira type cross-coupling of nitrobenzenes with terminal alkynes. *Chemical Communications*, 56(5):790-793, 2020.
- [19] Okita, T., Asahara, K. K., Muto, K., and Yamaguchi, J. Palladium-catalysed Mizoroki–Heck reaction of nitroarenes and styrene derivatives. *Organic Letters*, 22(8):3205-3208, 2020.

- [20] Isikgor, F. H. and Becer, C. R. Lignocellulosic biomass: a sustainable platform for the production of bio-based chemicals and polymers. *Polymer Chemistry*, 6(25):4497-4559, 2015.
- [21] Yan, J., Oyedele, O., Leal, J. H., Donohoe, B. S., Semelsberger, T. A., Li, C., Hoover, A. N., Webb, E., Bose, E. A., Zeng, Y., Williams, C. L., Schaller, K. D., Sun, N., Ray, A. E., and Tanjore, D. Characterizing variability in lignocellulosic biomass: a review. *ACS Sustainable Chemistry & Engineering*, 8(22):8059-8085, 2020.
- [22] a) Fortunati, E., Yang, W., Luzi, F., Kenny, J., Torre, L., and Puglia, D. Lignocellulosic nanostructures as reinforcement in extruded and solvent casted polymeric nanocomposites: an overview. *European Polymer Journal*, 80:295-316, 2016; b) Yu, S., Sun, J., Shi, Y., Wang, Q., Wu, J., and Liu, J. Nanocellulose from various biomass wastes: Its preparation and potential usages towards the high value-added products. *Environmental Science and Ecotechnology*, 5:100077, 2021.
- [23] a) Wathelet, B., Wathelet, B., and Jimenez-Araujo, A. Valorisation of pomegranate peel from 12 cultivars: dietary fibre composition, antioxidant capacity and functional properties. *Food Chemistry*, 160:196-203, 2014; b) Bhattacharjee, P., Dewan, A., Boruah, P.K., Das, M.R. and Bora, U. Pd (0)-embedded-lignocellulosic nanomaterials: A bio-tailored reusable catalyst for selective C2-H arylation of free N-H indoles. *Sustainable Chemistry and Pharmacy*, 33:101087, 2023.
- [24] White, R. J., Luque, R., Budarin, V.L., Clark, J. H., and Macquarrie, D. J. Supported metal nanoparticles on porous materials. Methods and applications. *Chemical Society Reviews*, 38(2):481-494, 2009.
- [25] Knossalla, J., Paciok, P., Göhl, D., Jalalpoor, D., Pizzutilo, E., Mingers, A.M., Heggen, M., Dunin-Borkowski, R.E., Mayrhofer, K. J. J., Schüth, F., and Ledendecker, M. Shape-Controlled Nanoparticles in Pore-Confined Space. *Journal of the American Chemical Society*, 140 (46):15684-15689, 2018.
- [26] Ndolomingo, M. J., Bingwa, N., and Meijboom, R. Review of supported metal nanoparticles: synthesis methodologies, advantages and application as catalysts. *Journal of Material Science A*, 55(15):6195-6241, 2020.

[27] Pacchioni, G., and Freund, H. J. Controlling the charge state of supported nanoparticles in catalysis: lessons from model systems. *Chemical Society Reviews*, 47 (22):8474–8502, 2018.

[28] Tursi, A. A review on biomass: importance, chemistry, classification, and conversion. *Biofuel Research Journal*, 6 (2), 962–979, 2019.

[29] a) Roglans, A., Pla-Quintana, A. and Moreno-Manas, M. Diazonium salts as substrates in palladium-catalysed cross-coupling reactions. *Chemical Reviews*, 106(11):4622-4643, 2006; b) Sengupta, S. and Bhattacharyya, S. Palladium-Catalysed Cross-Coupling of Arenediazonium Salts with Arylboronic Acids. *The Journal of Organic Chemistry*, 62(10):3405-3406, 1997; c) Darses, S., Jeffery, T., Genet, J.P., Brayer, J.L. and Demoute, J.P. Cross-coupling of arenediazonium tetrafluoroborates with arylboronic acids catalysed by palladium. *Tetrahedron Letters*, 37(22):3857-3860, 1996; d) Zong, Y., Hu, J., Sun, P. and Jiang, X. Synthesis of biaryl derivatives via a magnetic Pd-NPs-catalysed one-pot diazotisation–cross-coupling reaction. *Synlett*, 23(16):2393-2396, 2012.

[30] Felpin, F.X. and Sengupta, S. Biaryl synthesis with arenediazonium salts: cross-coupling, CH-arylation and annulation reactions. *Chemical Society Reviews*, 48(4):1150-1193, 2019.

[31] Colleville, A. P., Horan, R. A., and Tomkinson, N. C. Aryldiazonium tetrafluoroborate salts as green and efficient coupling partners for the Suzuki–Miyaura reaction: from optimisation to mole scale. *Organic Process Research & Development*, 18(9):1128-1136, 2014.

[32] Roscales, S. and Csáky, A.G. Transition-metal-free C–C bond forming reactions of aryl, alkenyl and alkynylboronic acids and their derivatives. *Chemical Society Reviews*, 43(24):8215-8225, 2014.

[33] Zheng, X., Ding, J., Chen, J., Gao, W., Liu, M. and Wu, H. The coupling of arylboronic acids with nitroarenes catalysed by rhodium. *Organic Letters*, 13(7):1726-1729, 2011.

- [34] Zhang, J., Chen, J., Liu, M., Zheng, X., Ding, J. and Wu, H. Ligand-free copper-catalysed coupling of nitroarenes with arylboronic acids. *Green Chemistry*, 14(4):912-916, 2012.
- [35] Chen, J., Wang, X., Zheng, X., Ding, J., Liu, M. and Wu, H. Ligand-free copper-catalysed *O*-arylation of nitroarenes with phenols. *Tetrahedron*, 68(43):8905-8907, 2012.
- [36] Zamiran, F. and Ghaderi, A. Nickel-catalysed de-nitrative etherification of activated nitrobenzenes. *Journal of the Iranian Chemical Society*, 16(2):293- 299, 2019.
- [37] Wang, H., Yu, A., Cao, A., Chang, J. and Wu, Y. First palladium-catalysed denitrated coupling reaction of nitroarenes with phenols. *Applied Organometallic Chemistry*, 27(10):611-614, 2013.
- [38] Begum, T., Mondal, M., Borpuzari, M. P., Kar, R., Gogoi, P. K., and Bora, U. Palladium-on-Carbon-Catalysed Coupling of Nitroarenes with Phenol: Biaryl Ether Synthesis and Evidence of an Oxidative-Addition-Promoted Mechanism. *European Journal of Organic Chemistry*, 2017(22):3244-3248, 2017.
- [39] Kataky, S., Choudhury, B., Neog, G., Das, M.R. and Thakur, A.J. Pd Nanoparticles Supported on Luffa Sponge as a Heterogenous Catalyst for C– O and C– C Coupling Reaction: From Waste to Use. *ChemistrySelect*, 9(33):e202401558, 2024.
- [40] Chen, J.S., Vasiliev, A.N., Panarello, A.P. and Khinast, J.G. Pd-leaching and Pd-removal in Pd/C-catalysed Suzuki couplings. *Applied Catalysis A: General*, 325(1):76-86, 2007.
- [41] Mao, S. L., Sun, Y., Yu, G. A., Zhao, C., Han, Z. J., Yuan, J., and Liu, S. H. A highly active catalytic system for Suzuki–Miyaura cross-coupling reactions of aryl and heteroaryl chlorides in water. *Organic & Biomolecular Chemistry*, 10:9410-9417, 2012.